Deep structure of the southern Kerguelen Plateau (southern Indian Ocean) from ocean bottom seismometer wide-angle seismic data

S. Operto, Philippe Charvis

JOURNAL OF GEOPHYSICAL RESEARCH, VOL. 101, NO. B11, PAGES 25,077–25,103, NOVEMBER 10, 1996

Deep structure of the southern Kerguelen Plateau (southern Indian Ocean) from ocean bottom seismometer wide-angle seismic data

Stéphane Operto[1]

Unité mixte de recherche Géosciences Azur, Centre National de la Recherche Scientifique, Villefranche-sur-mer, France

Philippe Charvis

Unité mixte de recherche Géosciences Azur, Institut Français de Recherche Scientifique pour le Développement en Coopération (ORSTOM), Villefranche-sur-mer, France

Abstract. Wide-angle seismic data collected during the Kerguelen ocean bottom seismometer experiment provide the first images of the deep structure of the southern Kerguelen Plateau and support a new interpretation of the origin of the plateau. Velocity models based on travel time inversions and reflectivity synthetic seismograms show a 22-km-thick crust composed of ~1.6 km of sedimentary cover, ~5.3 km of upper crust, ~11.0 km of lower crust, and a 4- to 6-km-thick reflective zone immediately above Moho. Velocities in the upper crust (from 3.8-4.5 km/s at top to 6.0-6.5 km/s at bottom) are consistent with the basaltic nature of this layer, the top of which was sampled during the Ocean Drilling Program. Velocities in the lower crust increase continuously from 6.60 km/s at the top to 6.90 km/s at 19.5 km depth. The reflective zone at the base of the crust identified by wide-angle reflections is observed only along the NNW-SSE direction. It consists of alternating high- and low-velocity layers with an average velocity of 6.70 km/s in the NNW-SSE direction and ≥6.90 km/s in the perpendicular direction. Strong azimuthal anisotropy is also observed in the upper mantle with velocities of 8.60 and 8.00 km/s, in the NNW-SSE and E-W directions, respectively. The absence of high velocities at the base of the crust that characterizes many large-volume mafic provinces, the reflective lower crust, and anisotropy in upper mantle suggest that the southern Kerguelen Plateau represents a stretched continental fragment overlain by basaltic flows isolated from the Antarctic margin during the early opening of the Indian Ocean.

Introduction

Episodes of intense magmatism have emplaced large igneous provinces (LIPs) on continents, along volcanic passive margins, in areas covered by continental flood basalt, and in ocean basins where they are represented by oceanic plateaus, submarine ridges, and seamounts. LIPs are usually not clearly related to plate tectonics, but they are often interpreted as a consequence of enhanced melting due to a mantle plume. Continuous plume activity at or near a spreading axis (e.g., Iceland), as well as starting plumes, produce huge quantities of melt in short periods, accounting for LIP emplacement [Farnetani and Richards, 1994]. In some cases, LIPs might reflect variations of global earth dynamics as is suggested by the relation between the Cretaceous emplacement of major oceanic plateaus and variations in magnetic reversal frequency [Coffin and Eldholm, 1994; Larson, 1991]. The study of LIPs is directly related to the understanding of mantle dynamics and associated magmatic processes. Numerical models of melt generation associated with mantle plume allow prediction of melt composition [Farnetani and Richards, 1994; White et al., 1992] and suggest that the seismic structure of the crust and upper mantle is a good indicator of the magmatic processes associated with the emplacement of oceanic plateaus.

The submarine Kerguelen Plateau in the Indian Ocean is known as one of the largest oceanic plateaus in the world, after the Ontong-Java plateau in the western Pacific, and thus is ideal for the investigation of LIP formation. Until recently, very little was known about the deep structure of the southern Kerguelen Plateau. The few existing multichannel seismic (MCS) lines only image the sedimentary cover and the uppermost part of the basement [*Coffin et al.*, 1990; *Rotstein et al.*, 1992; *Schaming and Rotstein*, 1990], and four Ocean Drilling Program (ODP) drillings reach the basaltic basement of the Kerguelen Plateau. In this paper, we present the deep structure of the southern Kerguelen Plateau, inferred from travel time inversion and amplitude modeling of wide-angle seismic data recorded along two perpendicular profiles.

Geological Setting

The Kerguelen Plateau stretches from 46°S to 64°S in a NNW-SSE direction in the southern Indian Ocean (Figure 1). It is surrounded by the following oceanic basins: the Crozet Basin to the north, the Enderby Basin to the west, and the Australian-Antarctic Basin to the east. To the south, the 3500-m-deep Prin-

[1] Now at Ecole des Mines de Paris

Paper number 96JB01758.
0148-0227/96/96JB-01758$09.00

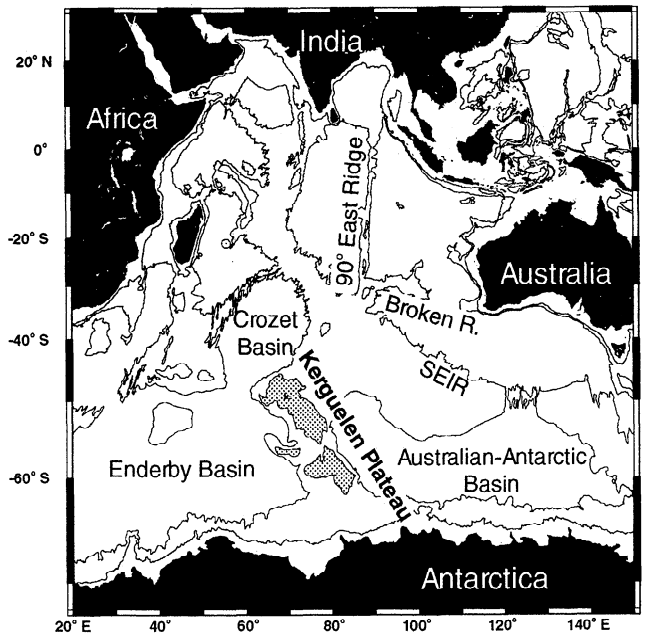

Figure 1. Bathymetric map of Indian Ocean from ETOPO-5 data [*National Geophysical Data Center*, 1988]. Only bathymetric contours 2000 and 4000 m are drawn. The top of the Kerguelen Plateau is shaded. SEIR indicates the southeast Indian Ridge.

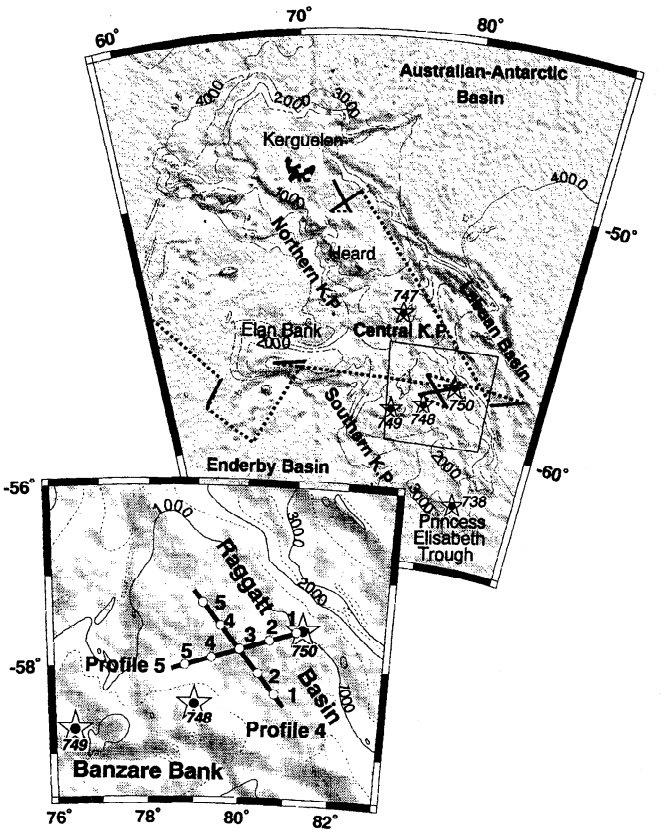

Figure 2. Bathymetric map of the Kerguelen Plateau after *Schlich et al.* [1987] modified using Kerguelen ocean bottom seismometer experiment (KeOBS) bathymetric data (polar stereographic projection). Contour interval is 1000 m. Shading corresponds to the satellite-derived, free-air gravity anomaly [*Sandwell and Smith*, 1994]. Tracks of the KeOBS experiment are indicated (dashed lines) and location of refraction profiles are marked by solid, thick lines. Stars mark locations of sites of Ocean Drilling Program (ODP) Legs 119 and 120, where basement was reached [*Schlich et al.*, 1989]. Inset shows detailed OBS positions along lines 4 and 5 (circles) shot in the Raggatt Basin.

cess Elisabeth Trough separates the Kerguelen Plateau from the Antarctic continental margin (Figure 1). The Kerguelen Plateau is usually divided into three major units, based on morphological differences: the northern, the central, and the southern Kerguelen Plateau [*Coffin et al.*, 1986; *Houtz et al.*, 1977] (Figure 2).

The southern Kerguelen Plateau, between 54° and 64°S, lies at an average water depth of 1500 m. A large sedimentary basin, the Raggatt Basin, lies in the eastern part of the southern Kerguelen Plateau, whereas the western part is occupied by a large volcanic structure, the Banzare Bank [*Coffin et al.*, 1990; *Rotstein et al.*, 1992]. Several N-S, NNW-SSE, and E-W tectonic features, resulting from extension or strike-slip faulting, affect this domain [*Angoulvant-Coulon and Schlich*, 1994; *Fritsch*, 1992; *Könnecke and Coffin*, 1995; *Munschy et al.*, 1993].

The western border of the southern Kerguelen Plateau is usually a gentle slope toward the deep Enderby oceanic basin. On the contrary, to the east, south of 48°S, the Kerguelen Plateau is bounded by a major fault scarp related to the rifting between the Kerguelen Plateau and Broken Ridge that culminated in breakup at 43 Ma (anomaly C18) [*Royer and Coffin*, 1992; *Royer and Sandwell*, 1989]. Before 43 Ma the Kerguelen Plateau and Broken Ridge formed a single LIP, the Cretaceous Kerguelen Plateau. South of 54°S, an area of tilted blocks, the Labuan Basin, bounds the eastern scarp of the Kerguelen Plateau. It is interpreted either as a stretched part of the southern Kerguelen Plateau or oceanic crust formed during the initial slow spreading at the eastern Indian Ridge [*Munschy et al.*, 1992; *Royer and Coffin*, 1992].

Seismic basement of the southern Kerguelen Plateau exhibits numerous dipping reflectors similar to those observed along volcanic passive margins [*Coffin et al.*, 1990; *Rotstein et al.*, 1992; *Schaming and Rotstein*, 1990]. The basement, sampled during ODP Leg 119 at Site 738 and ODP Leg 120 at Sites 747, 749 and 750 (Figure 2) [*Schlich et al.*, 1989]; consists of tholeiitic basalts, sometimes erupted in subaerial environment [*Salters et al.*, 1992; *Storey et al.*, 1992]. Nevertheless, *Ramsay et al.* [1986] and *Montigny et al.* [1993] reported that granitic debris, possibly ice rafted, was dredged in the southern Kerguelen Plateau and in the Labuan Basin.

Whole rock datings using the $^{40}Ar/^{39}Ar$ technique give ages of ~110 to ~114 Ma [*Whitechurch et al.*, 1992] for basalts recovered at Sites 749 and 750 in the southern Kerguelen Plateau. This is compatible with the plagioclase K-Ar age of 114 Ma obtained for basaltic sample dredged just to the north (Figure 2) [*Leclaire et al.*, 1987]. Basaltic basement at Site 747 as well as the basaltic flow reached at Site 748, are younger, 85 and 80 Ma, respectively [*Pringle et al.*, 1994].

Data

Experimental Overview

Seven wide-angle seismic lines were shot at sea in early 1991 on the Kerguelen Plateau and in adjacent oceanic basins during

the cruise 66 of the M/V *Marion Dufresne*, Kerguelen ocean bottom seismometer experiment (MD66/KeOBS). Lines 4 and 5 were shot in the Raggatt Basin, along NNW-SSE and E-W directions, respectively (Figure 2). More than 960 shots were recorded along each seismic line with a maximum source-receiver offset of 165 km and an average spacing between shots of ~185 m. Five ocean bottom seismometers (OBSs) were evenly deployed along each line. The central OBS (OBS 3) is located at the crossing point of lines 4 and 5 (Figure 2). Wide-angle seismic lines 4 and 5, were shot along MCS line RS47-24 of the R/V *Rig Seismic* and MCS line MD47-5 of the M/V *Marion Dufresne*, respectively [*Coffin et al.*, 1990; *Fritsch et al.*, 1992; *Rotstein et al.*, 1992]. OBS 1 of line 5 was deployed on the shallow drill Site 750 of the ODP Leg 120 [*Schlich et al.*, 1989].

The seismic source consisted of an untuned array of eight air guns, 16 L each (1000 in^3) fired simultaneously each 100 s (180-m spacing) at 140 bar of pressure (2000 psi) and operated by Groupement pour la Gestion de Navires Océanologiques, Institut Français de Recherche pour l'Exploitation de la Mer (GENAVIR–IFREMER). A hydrophone located 1 m over one of the air guns was used to trigger an OMEGA clock receiver to provide shot time log.

The receivers were three-component digital (4.5-Hz geophones) OBSs [*Nakamura et al.*, 1987]. The signal was sampled at a 10-ms interval with an antialias filter of 30 Hz. Data were recorded using a 20-s length window shifted with respect to the ship-receiver distance [*Nakamura et al.*, 1987]. Because of limited data storage capacity, horizontal components were usually recorded only at short ranges (≤25 km), whereas the vertical component was recorded along the entire profile. The exact locations of the OBSs on the bottom were computed using a least squares inversion of water wave travel times [*Nakamura et al.*, 1987]. A radio-controlled OMEGA clock receiver was used as a reference on board (accuracy of ±5 ms), and each OBS clock was corrected with respect to this reference.

Ship's location was recorded every minute using the non military channel of the Global Positioning System (GPS). Navigation data were plotted, and aberrant positions were removed and replaced by interpolated positions; navigation data were then smoothed using a three-point filter to obtain final fixes. The location of each shot was interpolated from the processed navigation log.

Processing

The data are band-pass-limited from 5 to 15 Hz with a dominant frequency of 8 Hz. The data were band-pass filtered using a zero phase Butterworth filter between 5 and 15 Hz during the travel time picking. The data were similarly filtered between 5 and 20 Hz for synthetic seismogram modeling. We used a spectral minimum phase deconvolution (whitening) to decrease source effect and to ensure accurate picking of travel times. Two-dimensional filtering in the frequency and wave number domains (FK filter) was used to attenuate water wave multiples from previous shots recorded at large offsets ("previous shot noise") and to recover postcritical travel times of reflections from the lowermost crust and Moho.

To enhance *PmP* imaging, we applied interspectral matrix filtering, allowing wave separation. It was performed by orthogonal projection of the data on the first eigenvector of the interspectral matrix constituted by the intercorrelation function between each seismic trace in the frequency domain [*Mari and Glangeaud*, 1990].

Modeling Strategies

The data were modeled using a two-dimensional (2-D) iterative, damped, least squares inversion of travel times [*Zelt and Smith*, 1992] and forward modeling of the amplitudes and waveforms using reflectivity synthetic seismograms [*Fuchs and Müller*, 1971]. We contoured the gross two-dimensional velocity model of the structure using travel time inversion and a stripping-layer approach proceeding from top to bottom of the structure. We complemented travel time inversion with preliminary amplitude modeling using zero-order asymptotic ray theory synthetic seismograms to estimate vertical gradients in the layers.

We estimate the uncertainty of a model parameter using a perturbation approach [*Zelt and Smith*, 1992]. The potential models must satisfy the following requirements: (1) The RMS misfit must not be significantly higher than the one computed during the inversion for the final model. (2) The model must allow rays to be traced to all the observed travel times. (3) Zero-order asymptotic ray theory amplitude must fit the observed amplitudes. The maximum perturbation of the parameter that allows a comparable fit to the observed data provides an estimate of its absolute uncertainty [*Zelt and Smith*, 1992].

Then, we computed synthetic seismograms using the reflectivity method to resolve finer details of the structure that could not be inferred from travel time analysis alone. The full reflectivity algorithm was required to model short-wavelength features located at the base of the crust. The assumption of one-dimensional (1-D) structure required by the reflectivity method was validated by computing travel times in the best fitting 1-D model. The 1-D velocity-depth function, interpolated beneath the OBS from the 2-D velocity model, was used as a starting model. We perturbed this velocity–depth function by a classical trial-and-error method to reach a satisfactory model. To complement qualitative (visual) comparison between the synthetic and real seismograms, we matched the maximum amplitude–distance curve measured by looking at the maximum amplitude in a short, wide window centered on the arrivals to be modeled.

The synthetic seismograms were computed at the same distances as the observed seismograms, keeping only one trace out of two. We applied the same processing (i.e., Butterworth filtering) to the synthetic seismograms and to the data in order to allow direct comparison of the two sets of seismograms. The synthetic seismograms were convolved with a minimum phase wavelet inferred from the spectral deconvolution of a set of traces centered on the water wave arrival. Vertical velocity gradients were approximated by a series of thin layers whose thicknesses were less than a quarter of the smallest wavelength.

Nomenclature

No shear waves were observed along lines 4 and 5. Thus, in the following, all the waves described refer to *P* waves.

The principal phases along lines 4 and 5 are (e.g., Figures 3a-3e): (1) refraction in the upper crust *Puc*, (2) refraction in the lower crust *Plc*, (3) reflection from Moho *PmP*, (4) refraction in the upper mantle *Pn*. Along line 4, two weak, wide-angle reflections are observed between the phases *Plc* and *PmP*. We interpret these arrivals as reflections from a reflective zone (RZ) located at the base of the crust between the lower crust (LC) and Moho (see following section for more details). We labeled *Pr1* the reflection from top of this reflective zone and *Pr* a reflection from within the RZ. Phases identified and the ranges over which they are observed are summarized in Table 1.

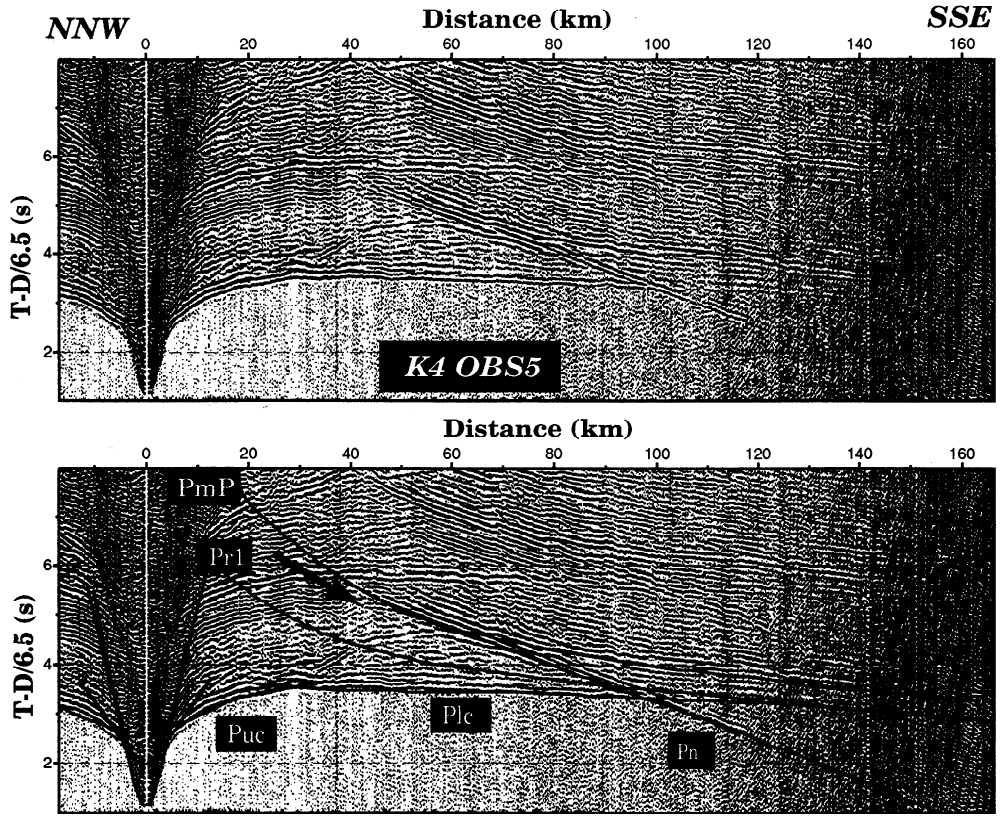

Figure 3a. (top) Record section from line 4 of ocean bottom seismometer (OBS) 5. (bottom) Travel time curves computed in the best fitting model (Figure 4) superimposed on the seismic section. Arrows indicate *Pr* reflections that are not modeled during travel times inversion. See Table 1 for nomenclature.

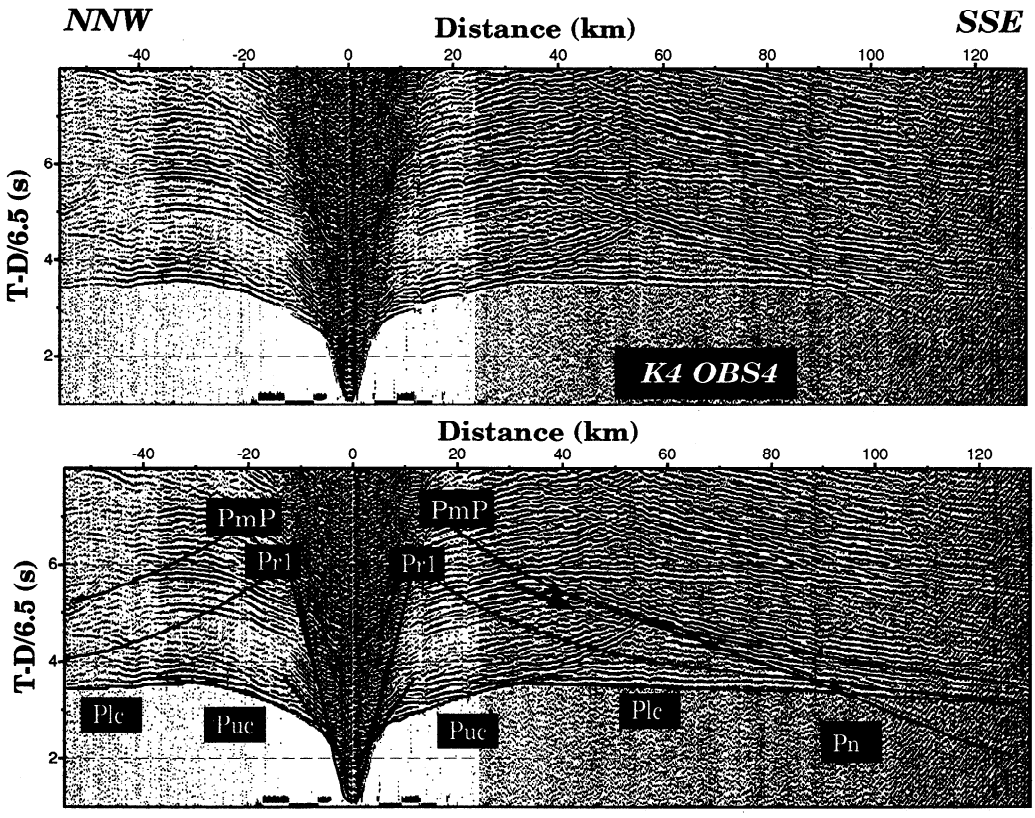

Figure 3b. Same as Figure 3a, but for OBS 4.

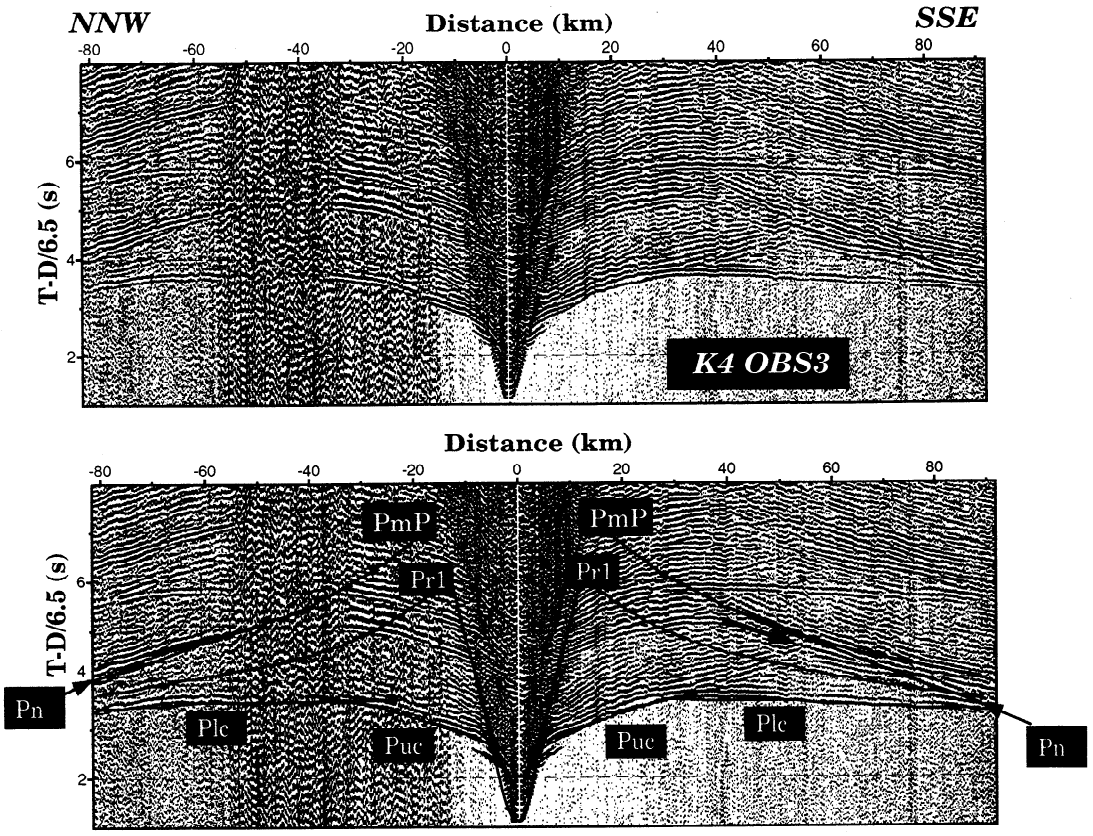

Figure 3c. Same as Figure 3a, but for OBS 3.

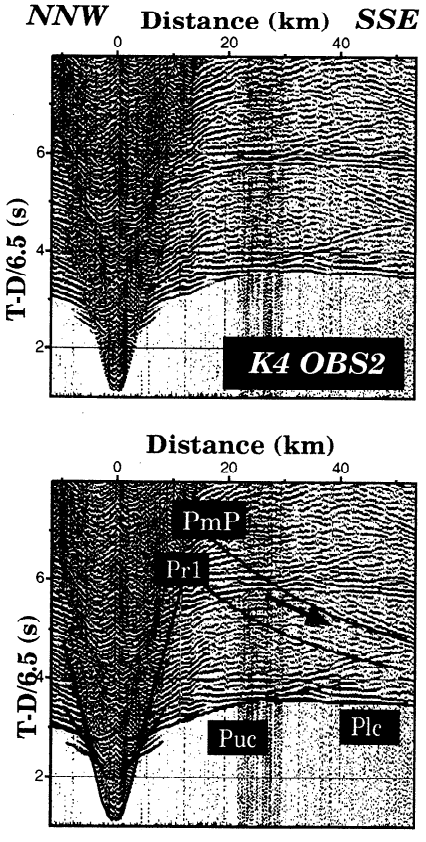

Figure 3d. Same as Figure 3a, but for OBS 2. Note that OBS 2 did not record a complete set of data due to technical problems.

Line 4

The final model inferred from travel time inversion for line 4 consists of following eight layers: water, three sedimentary layers, upper crust, lower crust, the reflective zone, and upper mantle (Figure 4). These layers were modeled using the inversion of the travel times of eight different phases (Table 2). The 2-D velocity model is complemented by two sets of 1-D velocity models inferred from reflectivity synthetic seismogram modeling for the crust down to the top of RZ (Figures 5 and 6) and for RZ, Moho and the upper mantle (Figures 7 and 8). The sedimentary cover is 1.0-2.3 km thick with velocities ranging from 1.7 to 3.4 km/s [*Operto*, 1995].

Upper Crust

During travel time modeling, the upper crust was modeled as a single layer with a vertical gradient, 4.5 to 6.5 km thick (Figures 4 and 5). Velocities at the top of the layer range from 5.0 to 5.2 km/s and velocities at the bottom range from 5.8 to 6.2 km/s. Vertical gradients range from 0.13 to 0.23 s^{-1}. Reflectivity synthetic seismograms contributed to point out several gradient discontinuities in the upper crust (Figure 5).

Lower Crust (Down to RZ)

During *Plc* travel time inversion, the lower crust is parameterized with no lateral variation. Both velocity at the top of the lower crust and vertical gradient (i.e., velocity at bottom of the lower crust) are involved during the travel time inversion in addition to the depth of the upper crust–lower crust interface. We

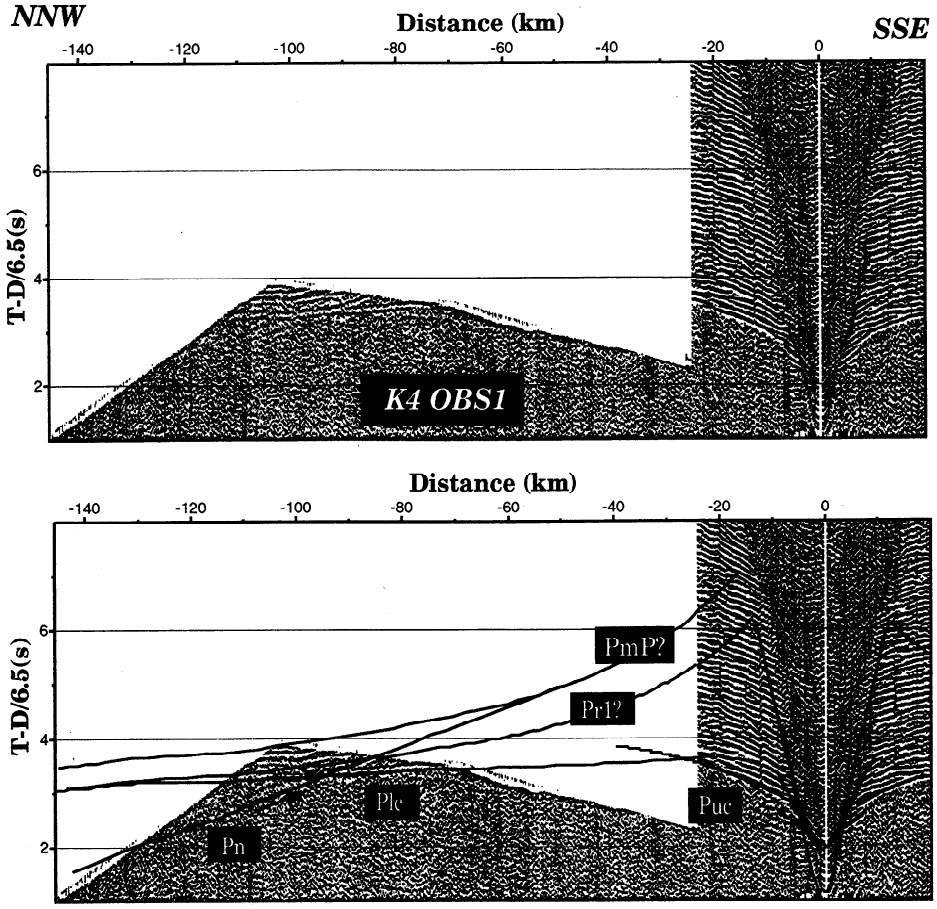

Figure 3e. Same as Figure 3a, but for OBS 4. Note that OBS 1 did not record a complete set of data for the same reason as OBS 2.

Table 1. Ranges Over Which Crustal and Mantellic Phases Are Recorded Along Lines 4 And 5

	OBS 1		OBS 2		OBS 3		OBS 4		OBS 5	
Phases	Left	Right	Left	Right	Left	Right	Left	Right	Left	Right
					Profile 4					
Pse	-4 to -8	4 to 8	-4 to -8	4 to 8	-4 to -8	4 to 8	-4 to -6	4 to 6	-4 to -7	4 to 7
Puc	-20 to -5	5 to 20	-20 to -5	5 to 15	-30 to -5	5 to 30	-30 to -5	5 to 30	-30 to -5	3 to 15
Plc		65 to 115	-55 to -20		-91 to -30	30 to 80	-130 to -30	30 to 55	-150 to -30	
Pre-PmP			-55 to -40		-65 to -40	50 to 60	-55 to -35		-65 to -35	
Post-PmP					-91 to -65	60 to 81	-130 to -55		-145 to -65	
Pn		80 to 95			-91 to -65	60 to 81	-115 to -55		-120 to -65	
Prl			-55 to -40		-90 to -40		-130 to -55		-135 to -50	
Pr			-55 to -40		-90 to -40		-130 to -55		-110 to -35	
					Profile 5					
Pse	-3 to -8	3 to 8	-4 to -9	4 to 9	-4 to -9	4 to 9	-3 to -6	3 to 6	-3 to -5	3 to 5
Puc	-16 to -3	3 to 20	-20 to -3	3 to 27	-30 to -5	5 to 30	-25 to -5	5 to 25	-27 to -5	5 to 17
Pruc	-6 to -12	6 to 12	-6 to -10	6 to 10						
Plc		20 to 140	-51 to -20	27 to 115	-90 to -30	30 to 75	-127 to -25	25 to 53	-140 to -27	
Pre-PmP		45 to 65		55 to 85	-90 to -50	50 to 75	? to -55		-85 to -55	
Post-PmP		65 to 140		85 to 115			-127 to ?		-140 to -85	
Pn				85 to 116					-100 to -85	

Ranges are provided for left side (negative values) and right side (positive values) of each ocean bottom seismometer (OBS) section (Figures 3 and 11). *Pse* is refraction in the sedimentary layers; *Pruc*, reflection from the top of the upper crust; *Puc*, refraction in the upper crust; *Plc*, refraction in the lower crust; pre-*PmP*, precritical reflection from the Moho; post-*PmP*, post-critical reflection from the Moho; *Pn*, refraction in the upper mantle; *Prl*, reflection from the top of the reflective zone (RZ); and *Pr*, internal reflection from the RZ.

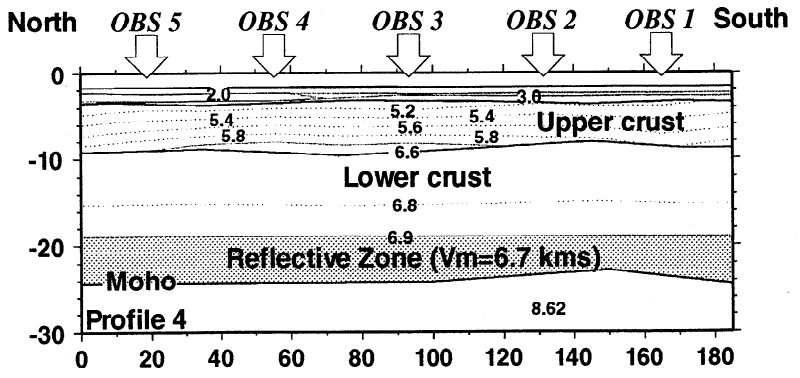

Figure 4. Best fitting velocity model across line 4 from two-dimensional (2-D) travel time inversion. Dotted curves are isovelocity contours with annotation (in kilometers per second). Solid curves delineate the main crustal layers (sedimentary layers, upper crust, lower crust, and reflective zone).

also tested the inversion by allowing lateral velocity variation and a reasonable constant vertical gradient of 0.035 s^{-1}. We obtained a similar RMS misfit for the *Plc* travel times with and without lateral velocity variation, proving that no lateral velocity variation is required by the data.

The depth to the top of the lower crust ranges from 8.8 to 9.6 km, the average velocity at the top of the lower crust is 6.64 km/s, and the vertical gradient in the lower crust computed during inversion ranges from 0.021 and 0.023 s^{-1} (these variations are due to geometry of the top of lower crust). On the basis of travel time analysis, gradients between 0.00 and 0.04 s^{-1} allow *Plc* travel time fits (Figure 6a), but amplitude analysis requires a gradient between 0.020 and 0.035 s^{-1} (Figure 6c). For gradients varying from 0.020 to 0.035 s^{-1}, velocities at a reference depth of 25 km in the lower crust vary between 7.00 and 7.20 km/s corresponding to an uncertainty of the lowermost crustal velocity of ±0.1 km/s (Figure 6a).

Similar velocity and gradients (6.65 km/s and 0.027s^{-1} respectively) were used during reflectivity synthetic seismogram modeling and allowed the simultaneous match of the travel times and amplitude of the *Plc* wave (Figure 5). The upper crust-lower crust interface must be modeled as a first-order discontinuity in order to explain the amplitude high located at 33 km of distance (Figure 5).

RZ, Moho, and Upper Mantle

The top of the RZ computed from the inversion of travel times of *Prl* does not exhibit significant dip and is located at 19.00 and 19.25 km depth for vertical gradients in the lower crust of 0.020 and 0.035 s^{-1}, respectively (Figure 4). The depth of the lower crust-RZ interface implies that velocity at the base of the lower crust is 6.89±0.1 km/s.

Internal seismic properties of RZ are not constrained by any refracted arrivals but only by a set of internal reflections, suggesting layering within the RZ (Figure 3). Consequently, RZ is parameterized as a homogeneous layer to derive the average properties of the media from travel time analysis (Table 2). More accurate parameterization (i.e., vertical and lateral variation) is not allowed because of (1) limitation of ray theory in the case of a heterogeneous structure, and (2) the small number of receivers available.

Table 2. Results of the Travel Time Inversion Along Lines 4 and 5

Phase	Layer	Ntobs	Nz	Nvs	Nvi	I	RMS, s	χ^2
		Profile 4						
Prse+ Pse	$Se_2(zv)+Se_3(z)$	240	9	9	0	2	0.060	9.000
Pruc+ Puc	UC(zv)	990	11	7	7	3	0.042	4.500
Plc	LC(zv)	1641	8	1	1	2	0.032	0.411
Prl	RZ(z)	632	5	0	0	1	0.047	0.223
PmP+Pn	RZ(v)+UM(zv)	1319	5	2	0	2	0.070	0.640
PmP+Pn	UM(zv) (wLVZ)	1321	5	1	0	1	0.117	1.156
		Profile 5						
Prse+Pse	$Se_2(zv)+Se_3(z)$	334	7	6	0	3	0.057	8.263
Pruc+Puc	UC(zv)	1125	13	7	7	2	0.058	8.276
Plc	LC(zv)	2547	7	1	1	2	0.054	1.172
Plc+PmP+Pn	LC(zv)+RZ(zv)+UM(zv)	3980	12	2	0	1	0.061	0.953
Plc+PmP+Pn	LC(zv)+UM(zv) (wLVZ)	4004	13	2	1	2	0.062	0.949

Phase is phase whose travel times are inverted. Detailled nomenclature is defined in Table 1 except Prse, internal reflection from the sedimentary cover. Layer refers to layers of the model perturbed during the inversion, z indicates that only the depth nodes are perturbed, v indicates that only the velocity nodes are perturbed and zv indicates that both depth and velocity nodes are perturbed; Se_i is sedimentary layer number *i*; UC, upper crust; LC, lower crust; RZ, reflective zone; UM, upper mantle, and wLVZ, no low velocity zone existing at the base of the crust. Ntobs is number of observed travel times used during the inversion, Nz is number of depth nodes computed during the inversion, Nvs is number of upper velocity nodes computed during the inversion, Nvi is number of lower velocity nodes computed during the inversion, I is number of iterations performed to compute the best fitting model, RMS is RMS misfit, and χ^2 is the corresponding chi-squared value.

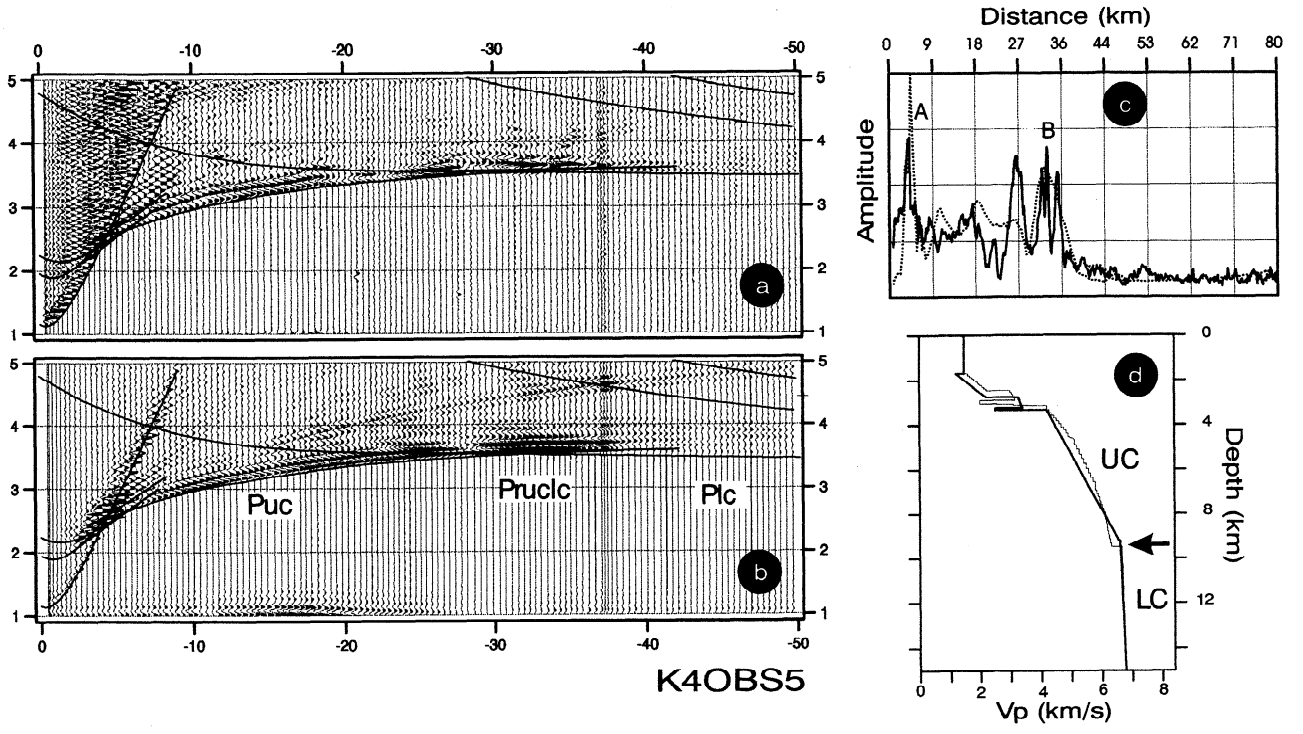

Figure 5. (a) Record section compared to (b) reflectivity synthetic seismogram section for OBS 5 along line 4. (c) Predicted (dotted curve) and observed (plain curve) maximum amplitude distance curves for the first arrivals. Amplitude peak labeled A marks the sediment-basement reflection and is generally overestimated from our modeling; B marks the upper crust-lower crust reflection. (d) One-dimensional (1-D) model deduced from reflectivity synthetic seismogram modeling (thin curve) and velocity-depth curve beneath OBS 5 in the best fitting model deduced from travel time inversion (thick curve) (Figure 4).

The average velocity in the RZ, computed at the same time with Moho depth and upper mantle velocity from simultaneous inversion of *PmP* and *Pn* travel times, is 6.70 km/s, with an uncertainty of 0.1 km/s (Figure 6b). Thus RZ constitutes a low velocity zone at the base of the large-scale crustal velocity structure (Figure 4).

We also test a model without RZ (i.e., with the lower crust down to the Moho). Inversion for this model led to a RMS misfit for *PmP* and *Pn* travel times as large as 0.117 s, instead of 0.070 s for the model with RZ (Table 2). This increase of the RMS misfit for the model without RZ is due to a delay between predicted and observed postcritical *PmP* travel times, whereas the existence of RZ at the base of the crust has little influence on the Moho depth that is mainly constrained by precritical *PmP* [*Operto and Charvis*, 1995].

Moho does not exhibit significant dip at depths ranging from 23.0 to 24.3 km, leading to a thickness of ~4-5 km for RZ (Figure 4). A near planar and horizontal Moho agrees well with the fact that precritical *PmP* and *Pn* travel times are comparable for OBS 3, 4, and 5 along line 4 (Figure 3). Nevertheless, the detailed shape of the Moho cannot be inferred unambiguously from travel time modeling as we assumed a laterally homogeneous RZ, whereas it is probably heterogeneous (discussed later). Thus we cannot discard the possibility of a gentle slope along the profile (that is, travel time inversion with a laterally heterogeneous RZ would lead to different Moho depths).

The velocity computed in the upper mantle is 8.60 km/s. This velocity is very high, but if we set the upper mantle velocity to 8.2 km/s (with a dipping Moho) the RMS misfit of *PmP* and *Pn* travel times is 0.115 s versus 0.070 s for the best fitting model (Table 2). Moreover, the Moho depth at the intersection between the two lines is in disagreement with the results obtained along line 5.

Using reflectivity synthetic seismograms, we tried to resolve some properties of the internal structure of RZ, at a scale within reach of the bandpass of the data. Data recorded along the two perpendicular directions suggest that RZ is a three-dimensional structure. Nevertheless, two criteria validate the use of a 1-D reflectivity method: (1) Ray tracing in our best fitting 1-D model allows us to match *PmP* and *Pn* travel times, validating the 1-D assumption at the scale of our modeling. (2) For one OBS, rays corresponding to the postcritical *PmP* (observed between 65 and 130 km of distances) reflect over a relatively narrow range of distances (between ~45 and 75 km). We identify two weak, wide-angle reflections (*Pr1* and *Pr*) observed on OBS 2, 3, 4, and 5 sections. These reflections are coherent over ~40 km of distance, with similar travel times and amplitudes on each section. This suggests that (1) the lateral extent of the reflectors associated with the *Pr1* and *Pr* waves is at least 30 km (roughly estimated by ray tracing for *Pr1* wave) and (2) *Pr1* and *Pr* waves reflect from significant geological boundaries located on top and near the base of the RZ, respectively.

Information we can infer from modeling of our data depends on the heterogeneity of the RZ and the band pass of the data. *Levander and Holliger* [1992] showed that in the case of a highly heterogeneous medium, the dynamic properties of the wave field are dominated by the small-scale variations of the physical properties as a result of strong scattering. The homogenization of the transmitted wave field through the heterogeneous medium (i.e., *PmP* wave) is illustrated by amplitude versus offset be-

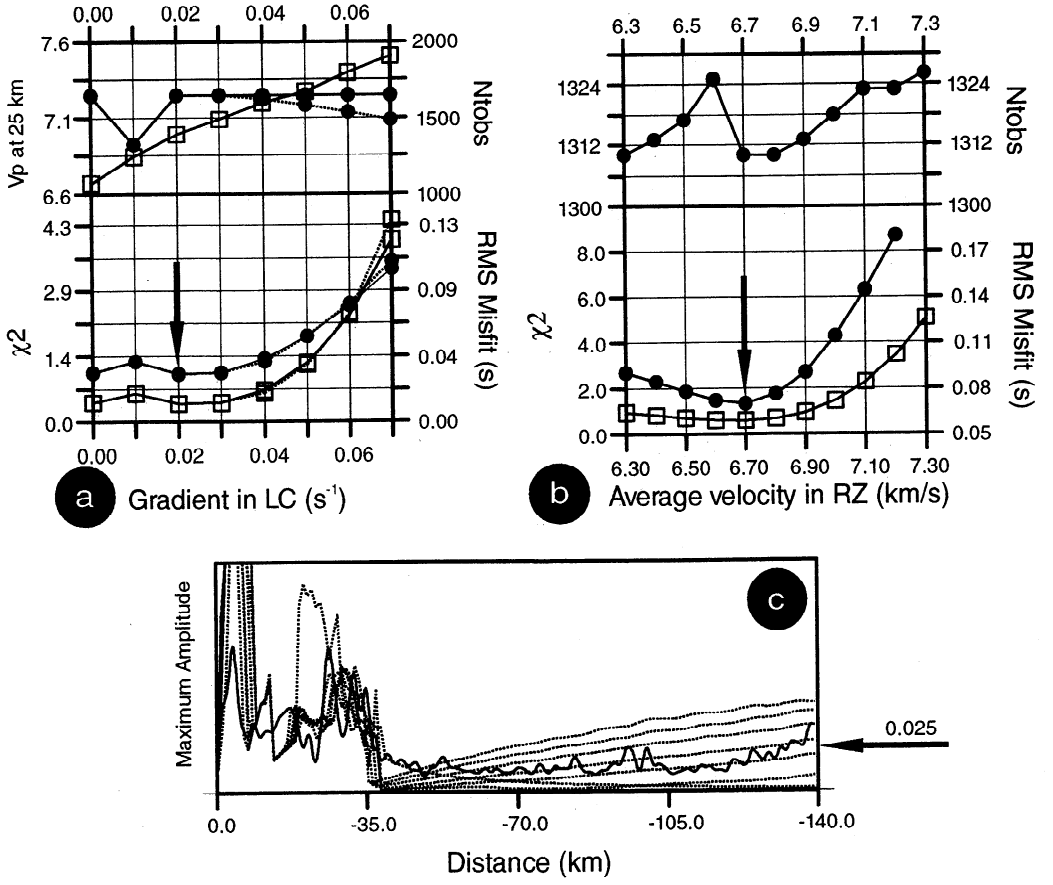

Figure 6. Analysis of uncertainty of the vertical velocity gradient in the lower crust and of the average velocity in the reflective zone (RZ) for profile 4. (a) Several parameters tabulated as a function of vertical velocity gradient in lower crust. (top) Number of observations (Ntobs) to which rays were successfully traced (circles), and velocity of P wave (Vp) at 25 km in the lower crust (squares). (bottom) RMS misfit between observed and computed travel times for the refraction in the lower crust (circles), and the corresponding chi-squared value, χ^2 [*Zelt and Smith*, 1992] (squares). The solid lines are for models with a lower crust thick enough to allow the rays to be traced to maximum number of observations, whereas dotted lines are for models with the base of the lower crust located at 20 km depth, corresponding approximately to the top of the RZ. Arrow indicates the best fitting vertical velocity gradient. (b) (top) Number of observations to which rays were successfully traced (circles) as a function of average velocity in the RZ. (bottom) RMS misfit between observed and computed Moho reflection and upper mantle refraction travel times (circles), and χ^2 (squares) as a function of average velocity in the RZ. (c) Observed (solid line) and predicted (dotted lines) maximum amplitude-distance curves of the *Plc* phase for OBS 5 of line 4. The predicted curves were computed by ray theory for seven values of the vertical velocity gradient: 0.00 (head wave), 0.01, 0.02, 0.03, 0.04, 0.05 and 0.06 s^{-1}. The reference amplitude is crudely provided by the maximum amplitude of upper crust-lower crust reflection located at ~30 km of range. The arrow indicates the best fitting vertical gradient (0.025 s^{-1}) that is consistent with the travel time analysis.

havior of the *PmP* characterized by lower amplitudes and a smoother pattern than the curve obtained for a homogeneous crust [*Levander and Holliger,* 1992, Figure 5]. This homogenization of the wave field implies that the large-scale velocity structure cannot be inferred unambiguously on the basis of seismic data in the case of a very heterogeneous lower crust. The amplitude versus offset curve of the *PmP* recorded by OBS 5 for line 4 suggests that the RZ is not heterogeneous enough to generate this homogenization, as a high critical amplitude of the *PmP* is observed (Figure 7a). On the contrary, RZ cannot be a homogeneous medium (or a layer with a constant vertical gradient) because this kind of structure would generate neither the wide-angle reflections from within the lower crust (Figure 8c) nor the sharp attenuation of the *PmP* postcritical amplitudes observed for OBS 5 of line 4 (Figure 7c).

Detailed modeling of the seismic properties of a layered media (i.e., thickness, number and impedance contrast between high- and low-velocity layers, extreme bounds of velocity in the layered structure, anelastic behavior of the lamellae) requires a broadband seismic record to study the low-pass-filtering effect of the layered media [*Paul and Nicollin*, 1989]. The spectral content of our data is mainly band-pass limited between 4 and 15 Hz. This lack of high frequency in the data spectrum is mainly related to the use of an untuned array of large air guns and precludes detailed modeling of the RZ seismic properties. Nevertheless, *Operto* [1995] noted that frequencies higher than 8 Hz seem to be attenuated between ranges of 50 and 70 km, where the wave field is dominated by *PmP* amplitudes. This may indicate frequency-selective attenuation of the transmitted wave field through RZ, with the lower limit of the attenuated frequency band equal to 8

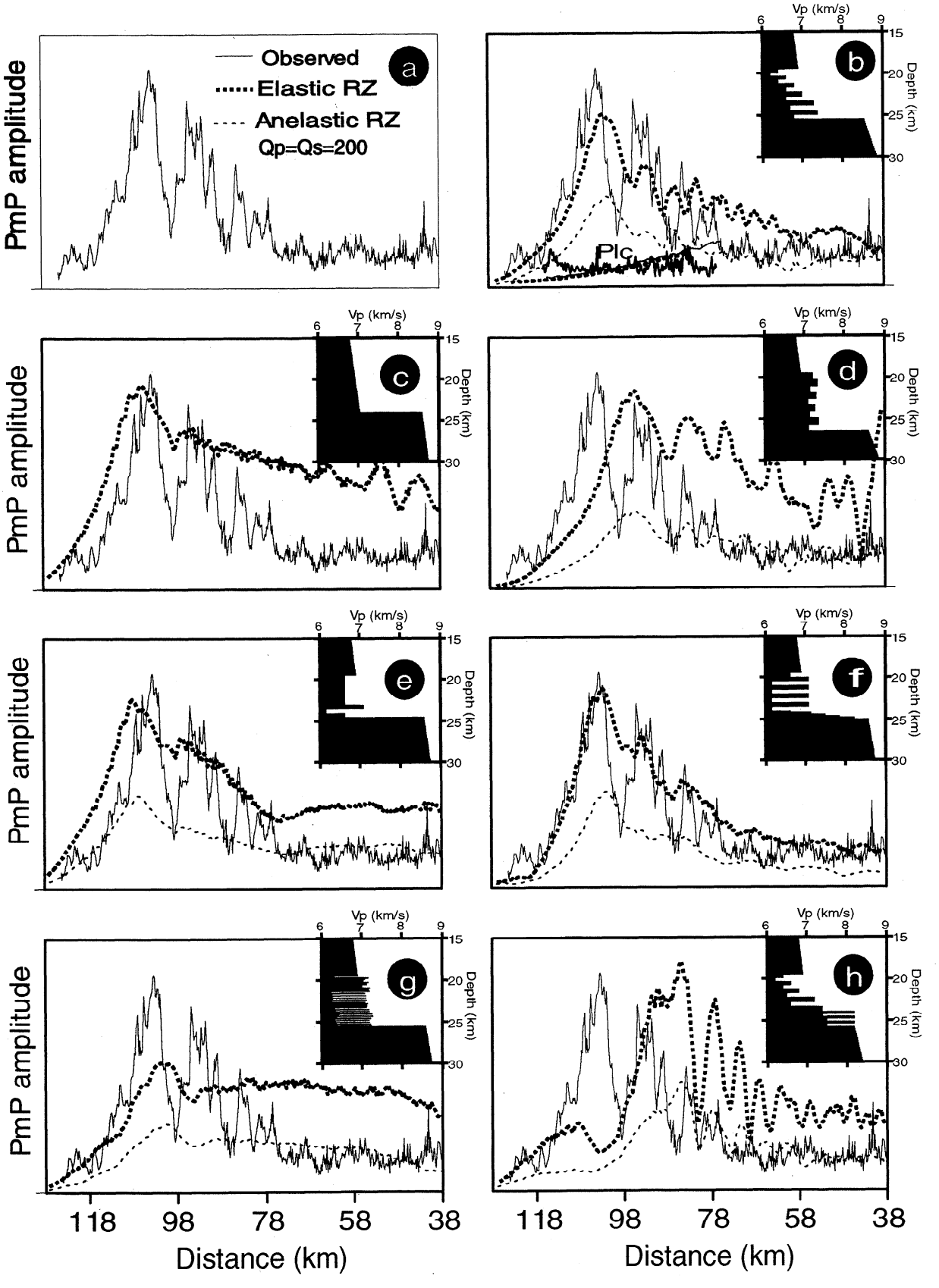

Figure 7. (a) Observed amplitude versus distance curves of the *PmP* recorded on OBS 5 along line 4. (b)-(h) Comparison between observed (solid curve) and predicted (dotted curve) amplitude of the *PmP*. The predicted amplitude is computed for the velocity–depth model of the RZ shown in the inset of each panel. Thick and thin dotted curves correspond to elastic RZ and anelastic RZ, respectively (Qp=Qs=200 in each lamellae). Amplitudes of the observed and synthetic *Plc* wave shown in Figure 7b were used as a reference.

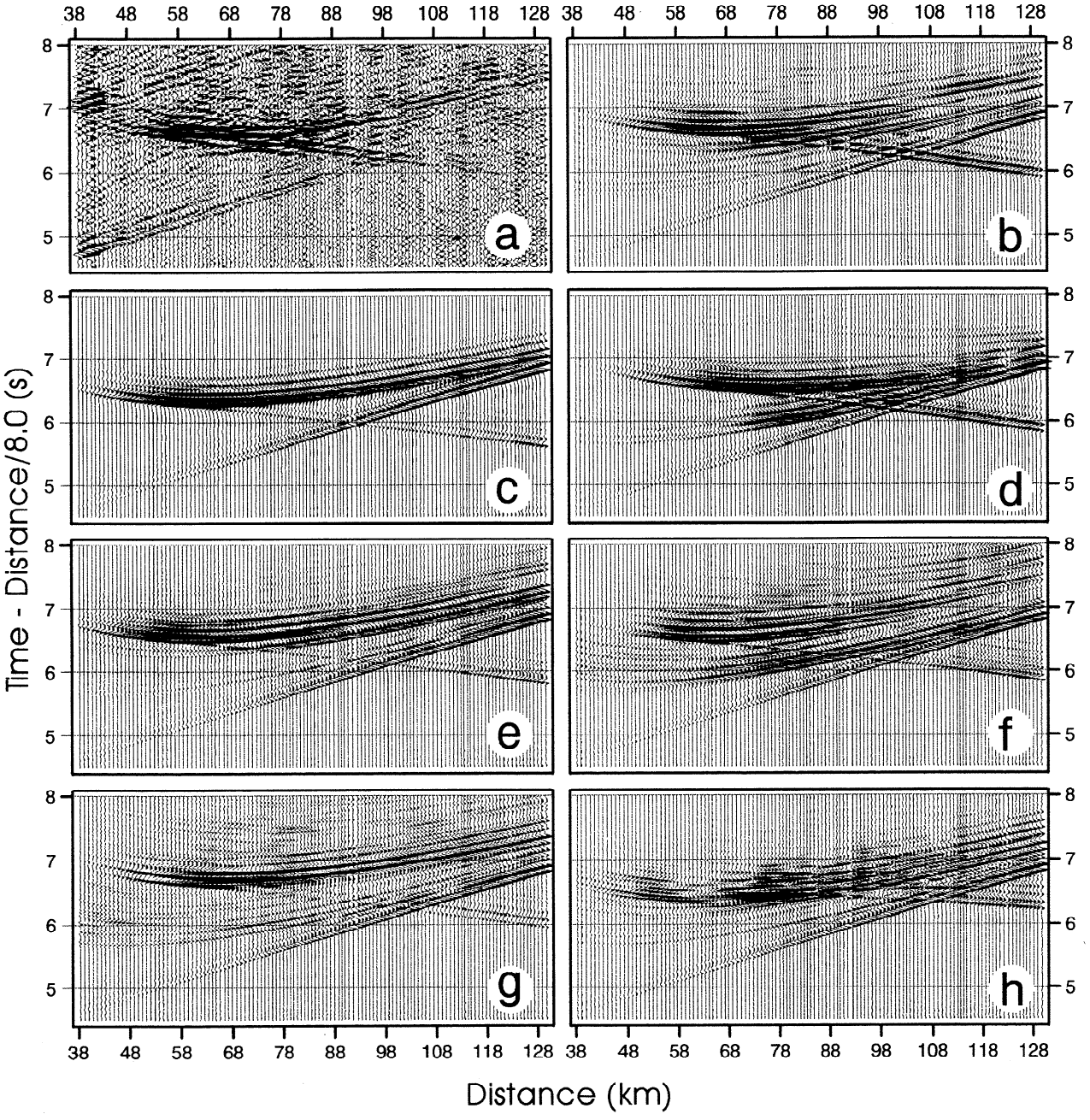

Figure 8. (a) OBS 5 record section (line 4) compared to (b)-(h) reflectivity synthetic sections computed for models shown in Figure 7b-7h.

Hz, whereas the upper limit of the attenuated frequency band is not recorded due to the lack of high frequencies. This lower-limit frequency constrains the lower bound of layer velocities, the upper bound of thickness distribution, and mainly, the impedance contrasts between layers [*Paul and Nicollin*, 1989].

Thus the objective of our modeling is not to infer the detailed internal structure of RZ but, rather, to give a rough estimate of the scale of the layering into RZ and to delineate some significant discontinuities into the RZ. We focus on modeling of a section recorded by OBS 5, and we will address more qualitative interpretation concerning the lateral variability of RZ along line 4.

Models with no low-velocity zone at the base of the crust are precluded because travel times and amplitude of the postcritical *PmP* do not fit the data (Figures 7c, 7d, 8c, and 8d). A model with a homogeneous RZ that encompasses the 500-m thick high-velocity (7.1 km/s) and low-velocity (6.3 km/s) lamellae (Figure 7e) produces a better fit between predicted and observed sections, although the postcritical *PmP* branch does not exhibit the discontinuous pattern of the observed section (Figure 8e) and has a higher amplitude (Figure 7e). With eight 500-m thick lamellae (Figure 7f), predicted and observed *PmP* look very similar (e.g., the discontinuous character of postcritical *PmP* is well mimicked) (Figure 7f and 8f), but amplitudes of *Pr* waves at pre-critical distances are too high on the synthetic section (Figures 8f). A model with thinner layering (~120-m-thick layers) (Figure 7g) is also precluded because amplitude does not match *PmP* (Figure 8g).

Our best fitting model, inspired by *Deichmann and Ansorge* [1983] (Figure 7b), consists of 600-m-thick lamellae with increasing impedance contrasts and decreasing vertical velocity gradients with depth. According to previous 2-D modeling, the average velocity in RZ is 6.70 km/s. We subdivided RZ into two main units: in the upper part of RZ, between depths of 19.5 and 23.3 km, velocities range between 6.40 and 7.00 km/s for the high-velocity layers and between 6.20 and 6.60 km/s for the low-velocity layers. Weak impedance contrasts between high- and low-velocity layers (between 0.030 and 0.056 km/s) allow generation of the weak amplitude of the reflections from the upper part of the RZ (Figure 8b). At 23.3 km depth, we delineate a more pronounced velocity step in RZ between 6.60 and 7.30 km/s that marks the top of the second unit in RZ (Figure 7b) and explain the higher amplitude of the identified *Pr* wave (Figure 8b). In the second unit of RZ, impedance contrasts between high- and low-velocity layers (0.080 km/s) are significantly higher compared with the upper part of the RZ. This increase of impedance contrast toward the base of RZ was required to generate enough attenuation of the *PmP* dominant frequency at postcritical distances related to short-path multiples in the lamellae (Figure 7b). Velocities range between 7.30 and 7.40 km/s for the high-velocity layers and between 6.70 and 6.80 km/s for the low-velocity layers. The absolute amplitude of *PmP* (Figure 7b) at critical distance is generated by a sharp first-order discontinuity at Moho between 6.80 and 8.60 km/s, although the presence of a layered Moho (Figure 7g) or a ~1-km-thick crust–mantle transition are not precluded (Figure 7d). We note also that travel times of intrabed multiples reflected from the top of the RZ and from the velocity step that delineates the two units in the RZ fit two wide angle reflections recorded after *PmP* (Figure 9).

We believe that the reflectivity of the RZ probably increase from north to south (from OBS 5 to OBS 1). The wave train of the *PmP* is clearly broader for OBS 4 than for OBS 5 (Figures 10a and 10b), and the maximum amplitude versus offset curve is more homogeneous for OBS 4 than for OBS 5 (Figure 10c). We interpret this as the result of increase scattering associated with a more heterogeneous (e.g., layered) RZ.

The distance at which *Plc* and *Pn* arrivals cross is smaller on OBS 1 (90 km) than on OBS 4 (92 km) and OBS 5 (98 km) sections, whereas upper and lower crustal travel times, as well as the apparent velocity of the *Pn* wave, are similar. This can be related to (1) a lower average velocity in the RZ southward, (2) a Moho dipping northward, or (3) a higher upper mantle velocity southward. The second and third hypotheses are unlikely because the apparent *Pn* velocity is similar on both sections and because these hypotheses would lead to an upper mantle velocity higher than 8.60 km/s. On the contrary, there may be a connection between the decrease of the average velocity in RZ from north to south and the increase of the heterogeneity of RZ from north to south. This connection would result from a longer ray path related to propagation in a more heterogeneous media [*Ojo and Mereu*, 1986]. Nevertheless, the variation of reflectivity from north to south remains highly speculative owing to the small number of receivers available.

Line 5

The final 2-D velocity model for line 5, based on the travel time inversion of seven different phases (Figures 11a-11e and Table 2), consists of eight layers (Figure 12) corresponding to the layers described along line 4. One-dimensional velocity models of the crust were inferred from reflectivity synthetic seismogram modeling.

Upper Crust

On the basis of travel time inversion, thickness of upper crust varies between 4.6 and 6.1 km and velocity varies between 4.80-5.00 km/s at the top and 5.50-6.20 km/s at the bottom of the

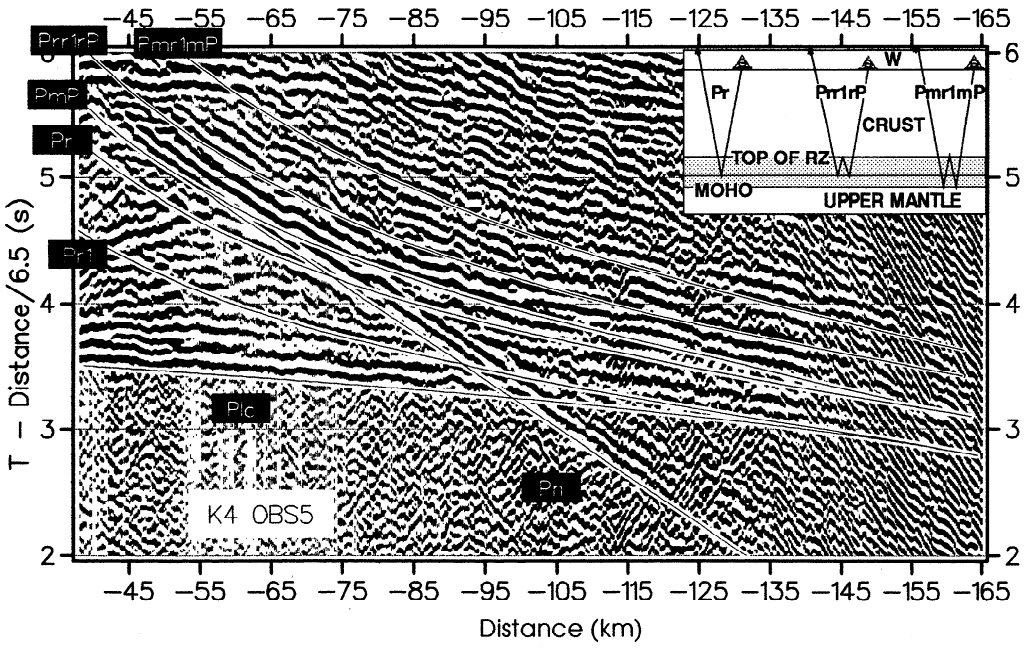

Figure 9. Detail of record section from OBS 5 for profile 4 centered on the *PmP* with superimposed travel time curves computed using 1-D ray tracing in the model of Figure 7b. Inset shows schematic ray path for the different interpreted arrivals.

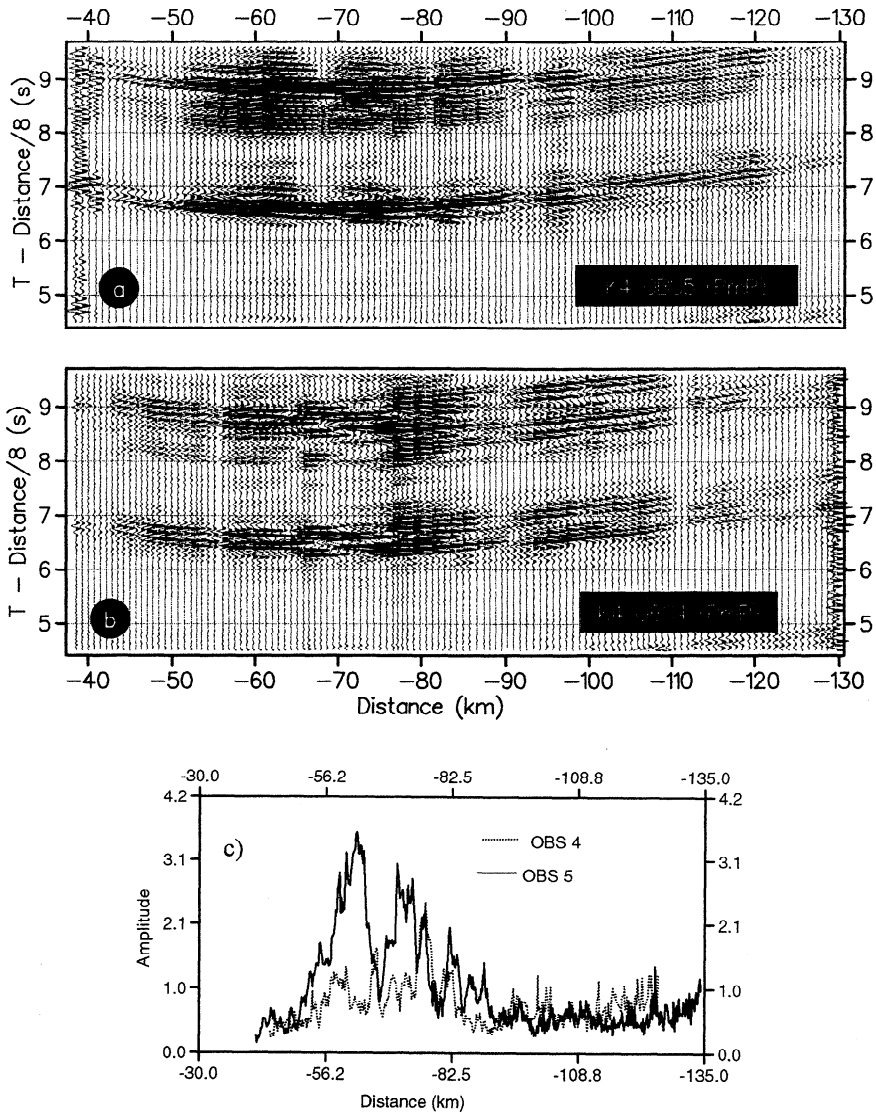

Figure 10. Comparison of the *PmP* for (a) OBS 5 and (b) OBS 4 along profile 4. *PmP* waves (and their multiples) were separated from the whole section using interspectral matrix filtering [*Mari and Glangeaud*, 1990]. (c) Amplitude of the *PmP* versus distance for OBS 5 (solid curve) and 4 (dotted curve) along line 4.

layer. Synthetic seismogram modeling of theOBS 1 record section required a velocity of 3.80 km/s at the top of the layer (Figure 13), near the basement high located along the flank of the basin. Beneath OBS 3, synthetic seismogram modeling reveals a local low velocity zone into the upper crust (Figure 14). Vertical velocity gradients are from 0.170 and 0.430 s^{-1}.

Lower Crust

The depth of the top of the lower crust ranges from 6.4 to 9.3 km. At the crossing point of lines 4 and 5, the mismatch (<0.2 km) is lower than the a priori uncertainty assigned to the depth parameter for this interface. The average velocity at the top of lower crust is 6.62 km/s, and the vertical gradient is between 0.024 and 0.029 s^{-1}, showing a good agreement with line 4. On the basis of synthetic seismogram modeling, the upper crust-lower crust interface constitutes a first-order discontinuity required to match the amplitude high at 23 and 31 km of distance for OBS 1 and 3, respectively (phase labeled *Pruclc*, Figures 13 and 14).

Vertical velocity gradients of 0.00 to 0.05 s^{-1} are consistent with the travel time analysis (Figure 15a), whereas amplitude analysis suggests that the gradient must be in the range of 0.02 to 0.04 s^{-1} (Figures 15b and 15c). These gradients yield velocities varying between 7.00 and 7.30 km/s at 25 km depth in the lower crust, corresponding to an uncertainty of the lowermost crustal velocity of ±0.15 km/s.

RZ, Moho, and Upper Mantle

Along profile 5, there is no evidence of RZ at the base of the crust, as no reflection *Pr* is observed, and the postcritical *PmP* travel time curve becomes asymptotic to the *Plc* travel time curve beyond 110 km. Nevertheless, we tested whether a model with a RZ at the base of the crust can account for the travel times observed along line 5 (Figure 12). The starting model had a RZ of a similar thickness in the middle of the basin (kept fixed during inversion) to that computed along line 4, and the Moho depth was kept fixed at 24.2 km in the middle of the basin during this tentative inversion. The fits between observed and computed

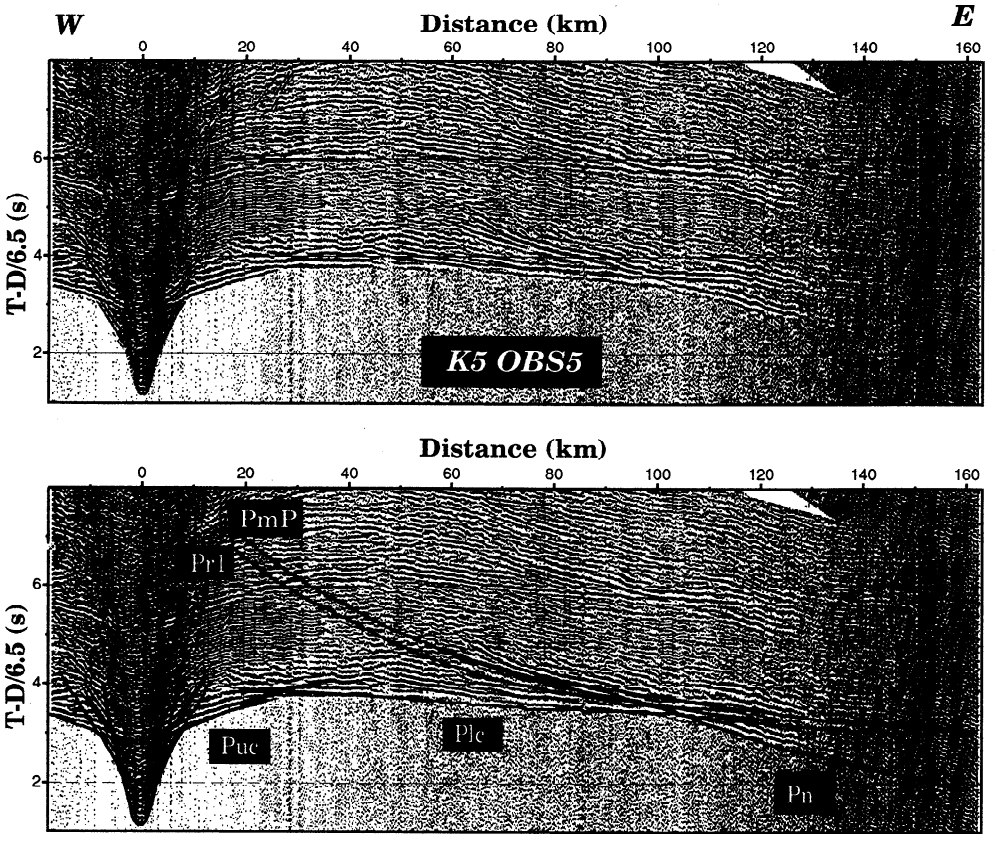

Figure 11a. (top) Record section from line 5 of OBS 5. (bottom) Travel time curves computed in the bestfitting model (Figure 12) superimposed on the seismic section. See Table 1 for detailed nomenclature.

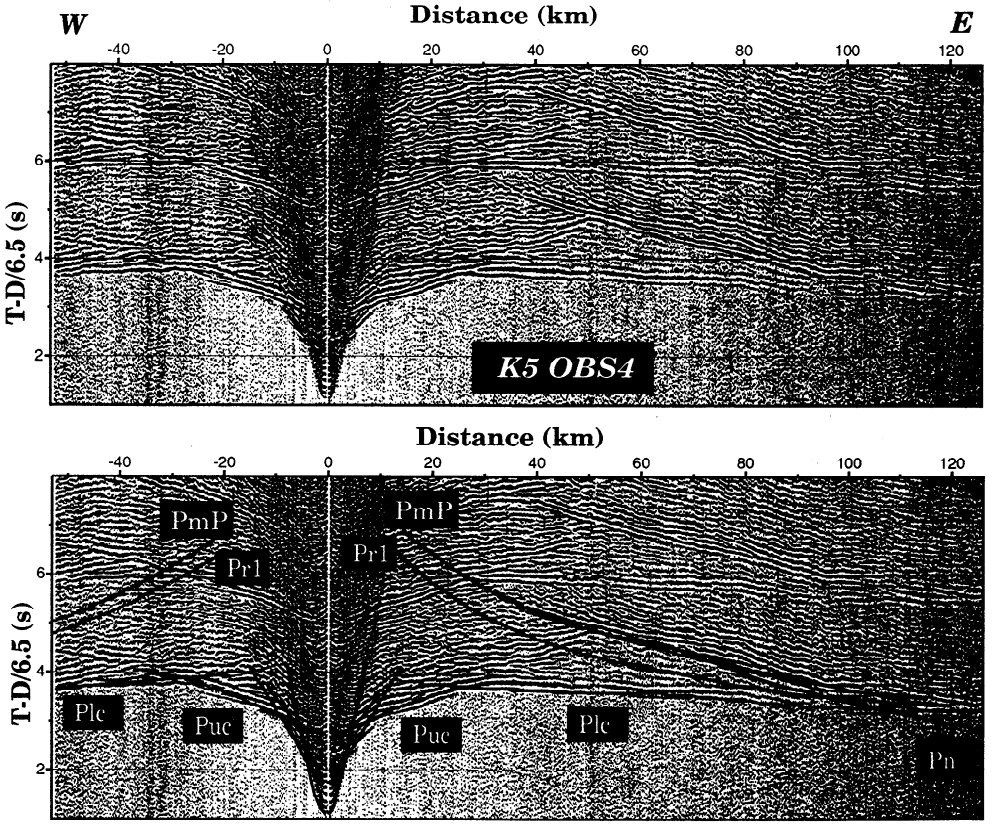

Figure 11b. Same as Figure 11a, but for OBS 4.

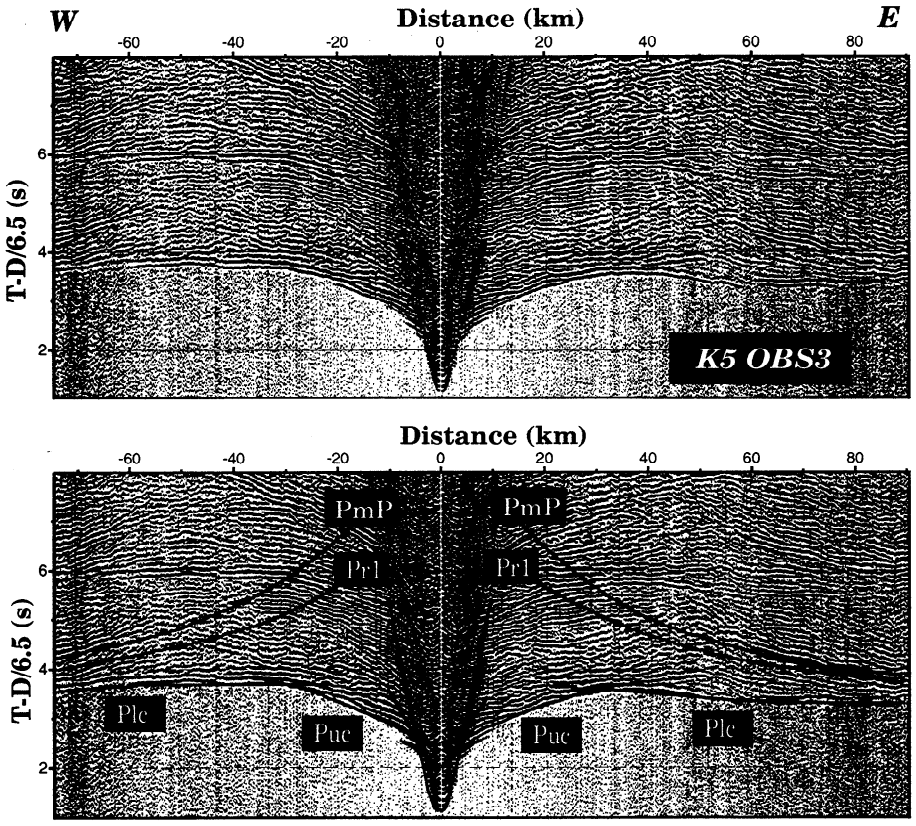

Figure 11c. Same as Figure 11a, but for OBS 3.

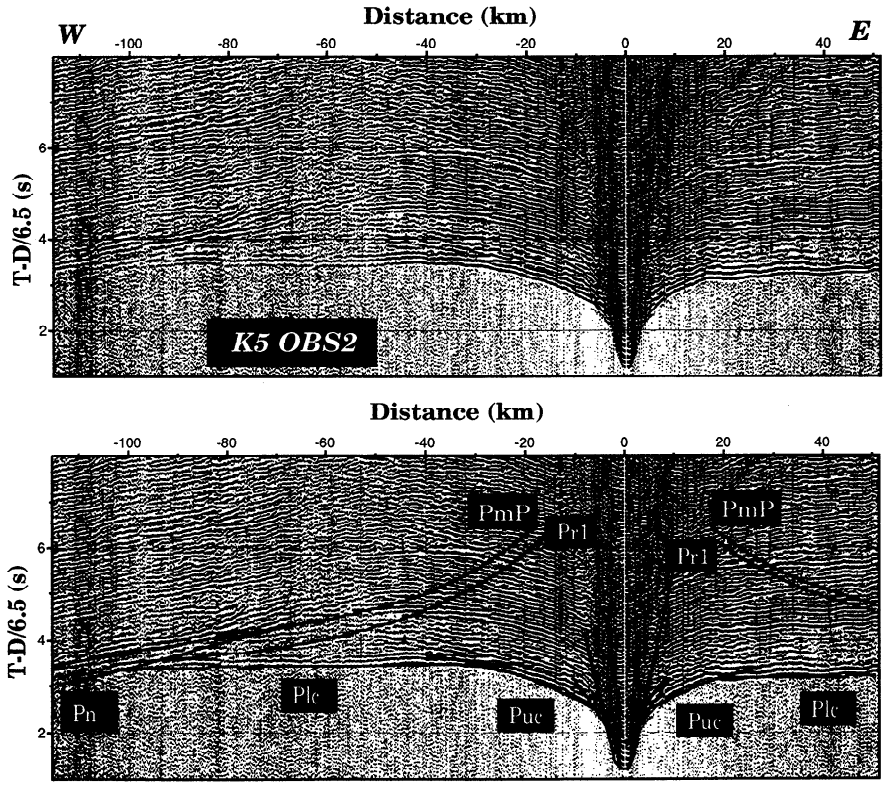

Figure 11d. Same as Figure 11a, but for OBS 2.

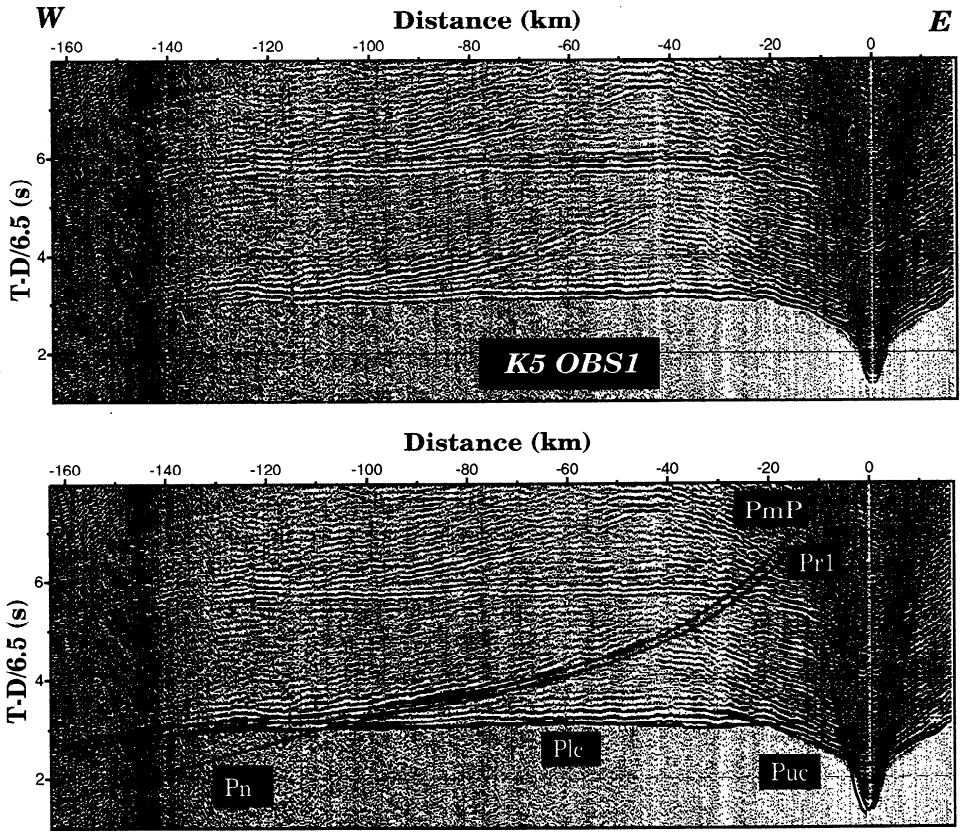

Figure 11e. Same as Figure 11a, but for OBS 1.

travel times and the ray coverage are similar for models with and without RZ (Table 2). The average velocity in the RZ is 6.90 km/s and thus is similar to the velocity at the base of the lower crust (which is in agreement with the asymptotic relation between the *Plc* and postcritical *PmP* along line 5). Moho depth ranges from 22.8 to 24.2 km. The velocity of 8.00 km/s, computed at the top of the upper mantle, is constrained by the *Pn* travel times visible on OBS 2 and OBS 5 in reversed locations. Zero-order asymptotic ray theory seismograms were computed in the 2-D velocity model to check the location of the critical distance between *PmP* and *Pn*. On the sections where no *Pn* is observed (i.e., OBS 1), we assume that the critical distance is located approximately at the location of the maximum amplitude of the *PmP*. This assumption is plausible, as the wave field seems not to be affected by the heterogeneous lower crust. Synthetic sections computed for OBS 5 (Figure 16) and OBS 1 (Figure 17) show that this feature is correctly modeled.

Integrated Model of Southern Kerguelen Plateau

The crust beneath the southern Kerguelen Plateau is 22 km thick, on average, with Moho lying at 23-24 km depth. Velocity models along lines 4 and 5 are similar down to ~19 km depth

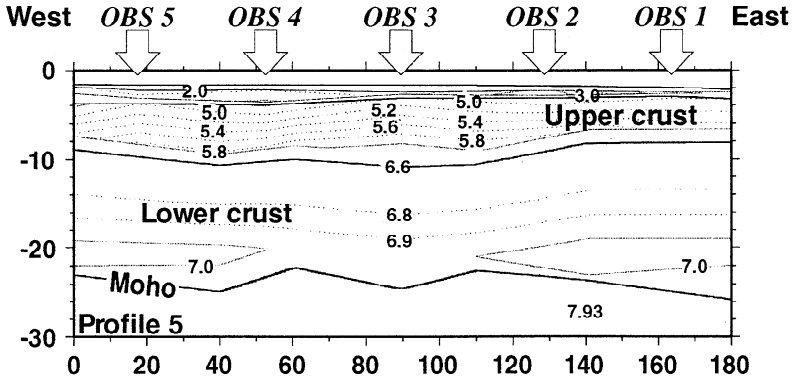

Figure 12. Best fitting velocity model across line 5 from 2-D travel time inversion. Dotted curves are isovelocity contours with annotation (in kilometers per second). Solid curves delineate the main crustal layers (sedimentary layers, upper crust, lower crust, and reflective zone).

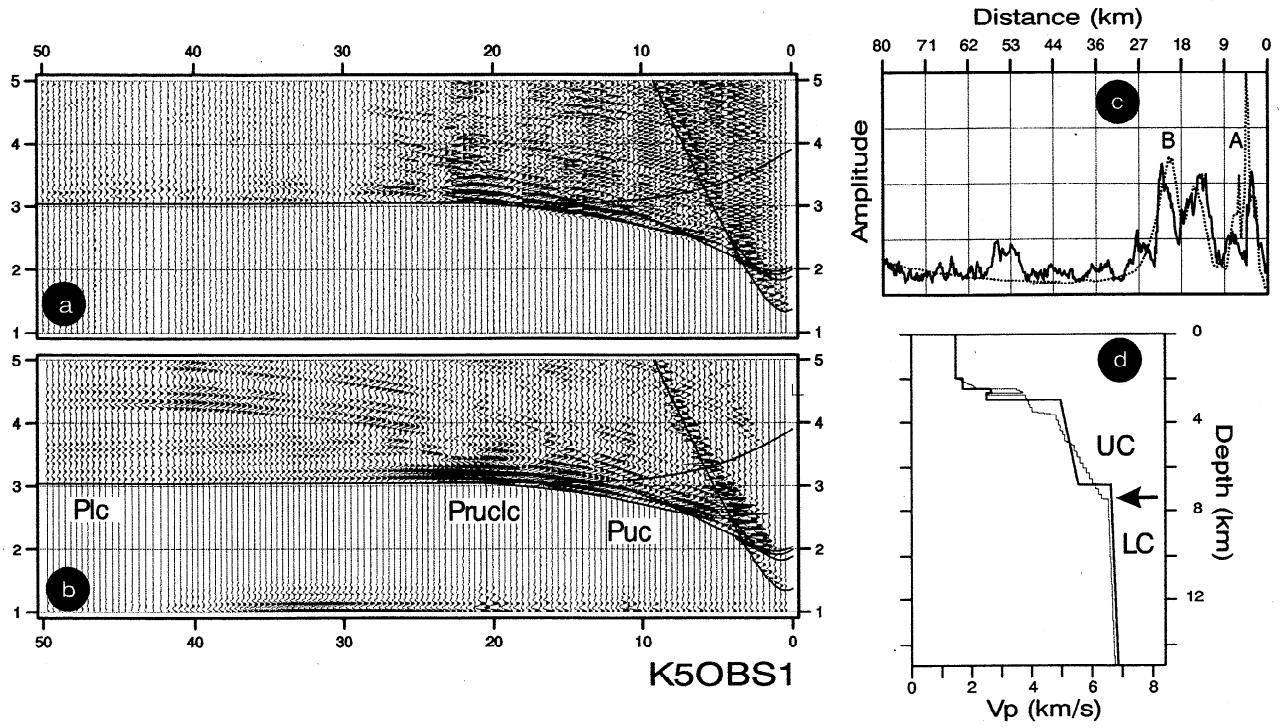

Figure 13. (a) Record section compared to (b) reflectivity synthetic seismograms section for OBS 1 along line 5. (c) Predicted (dotted curve) and observed (solid curve) maximum amplitude distance curves for the first arrivals. Amplitude peak labeled A marks the sediment-basement reflection and is generally overestimated from our modeling; B marks the upper crust-lower crust reflection. (d) One-dimensional model deduced from reflectivity synthetic seismogram modeling (thin curve) and velocity-depth curve beneath OBS 1 in the best fitting model deduced from travel time inversion (thick curve) (Figure 12).

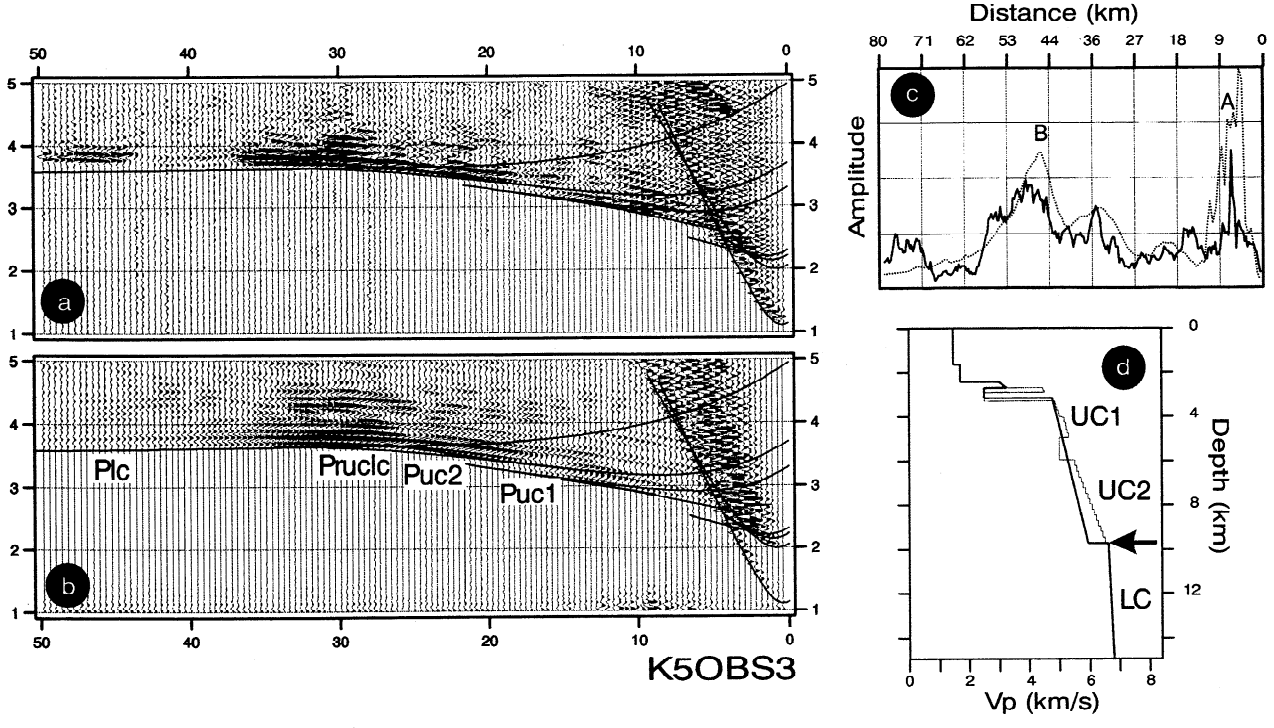

Figure 14. Same as Figure 13, but for OBS 3 along line 5.

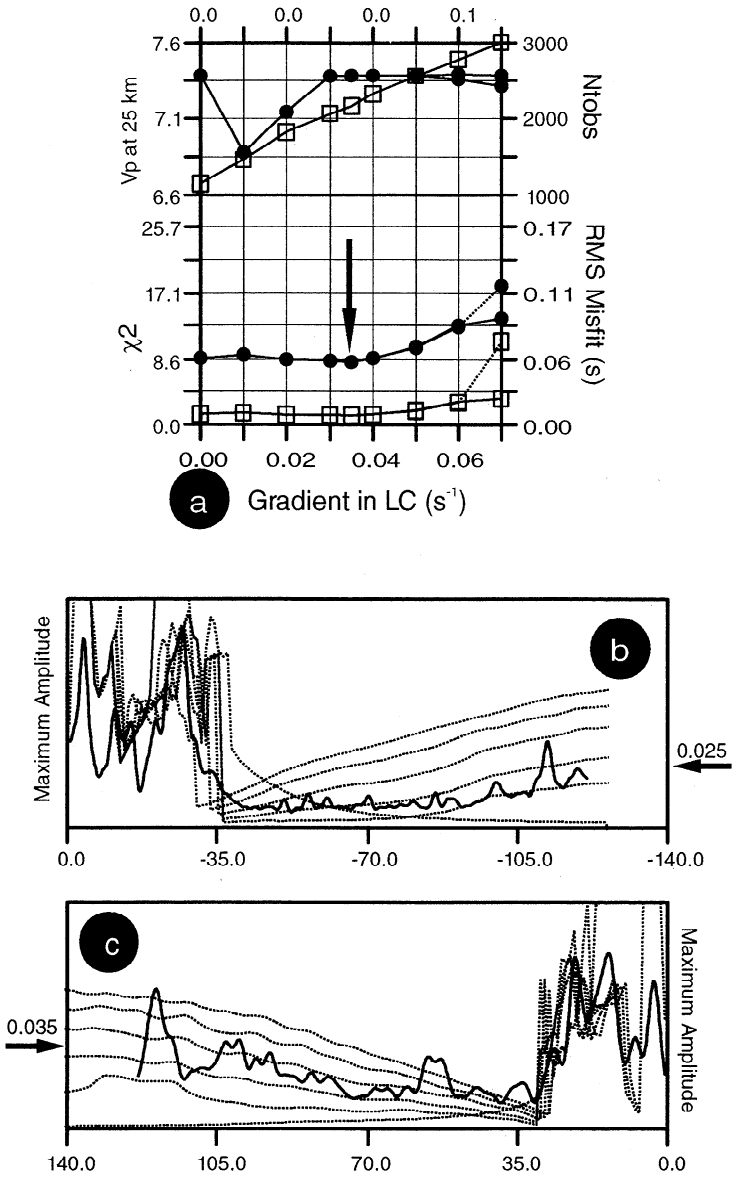

Figure 15. Analysis of uncertainty of the vertical velocity gradient in the lower crust. (a) Same as Figure 6a, but for line 5. (b) Same as Figure 6c, but for OBS 1, line 5. (c) Same as Figure 6c, but for OBS 5, line 5.

(i.e., down to the base of the LC), although sediment-upper crust and upper crust-lower crust interfaces have more relief along line 5, roughly perpendicular to the trend of the plateau. Gradient discontinuities and low-velocity layers in the upper crust are clearly not correlated from one OBS to another, suggesting that they constitute isolated and local features (compare 1-D velocity model of Figures 5, 13, and 14).

The base of the crust (i.e., RZ), the Moho, and the velocity in the upper mantle show striking differences along lines 4 and 5. Along line 4, the average velocity in RZ (inferred from travel time inversion of postcritical *PmP*) is 6.70 km/s, whereas it is at least 6.90 km/s along line 5. Layering of RZ along line 4 is identified by several wide angle reflections and the discontinuous pattern of the wave field at *PmP* postcritical distances. Along line 5, these features are not observed and RZ is seismically transparent. The azimuthal velocity anisotropy in RZ is probably connected with the difference in reflectivity in the two perpendicular directions (see interpretation in the following section). Velocities at the top of the upper mantle are 8.60 km/s along line 4 and 8.00 km/s along line 5, indicating a 8% azimuthal anisotropy with the fast direction close to the axis of the plateau.

Discussion

The lithospheric structure (down to the top of the upper mantle) of the southern Kerguelen Plateau shows unusual features for an oceanic plateau. High velocities at the base of the crust, related to magnesium-rich gabbros, that characterized thickened oceanic crust are not observed beneath the southern Kerguelen Plateau. Moreover, the reflectivity and the anisotropy of the lowermost crust described in the previous section are not typical of an oceanic crust that exhibits usually a more simple seismic pattern. For these reasons, we propose that the Raggatt Basin may consist of a fragment of continental crust, stretched in the

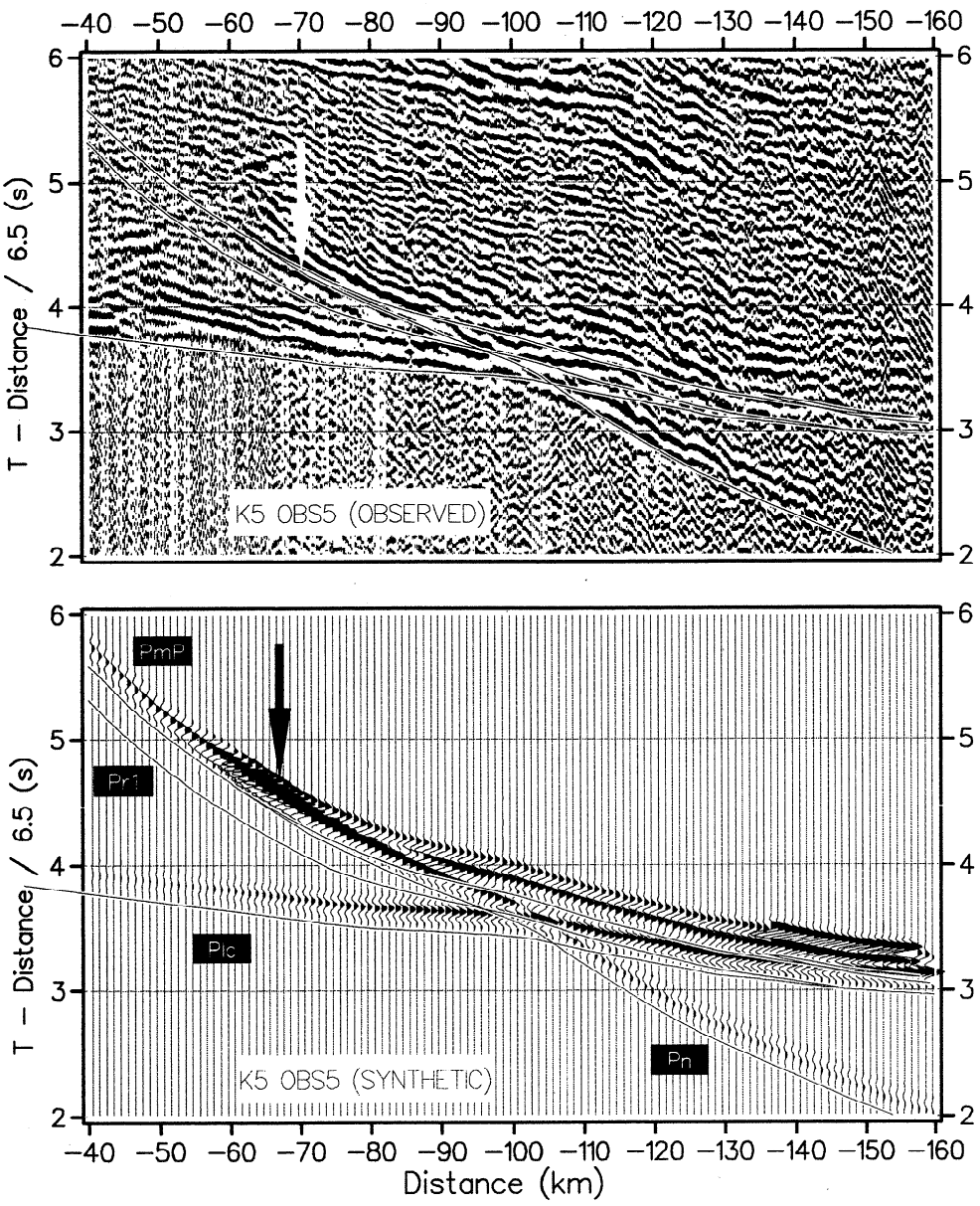

Figure 16. (top) OBS 5 record section centered on *PmP* compared to (bottom) zero-order asymptotic ray theory seismograms computed in the 2-D velocity model (Figure 12). The arrows indicate our interpretation of the critical distance identified by the maximum amplitude of *PmP*.

NNW-SSE direction and overlain and possibly intruded by magmatic material. The velocities of the lower crust, including layers LC and RZ, are in good agreement with the velocities observed in the lower continental crust beneath rifts and/or continental margins. The extension of the continental crust can explain the reflectivity of the base of the crust, as well as the anisotropy observed in the reflective lower crust and upper mantle. Before we develop the arguments for a continental origin, we review the arguments against an oceanic origin for the southern Kerguelen Plateau.

Is the Southern Kerguelen Plateau an Oceanic Plateau?

Most of the previous geophysical, geological, and geochemical studies on the southern Kerguelen Plateau suggest that it could be a pure oceanic plateau emplaced either in a setting similar to Iceland today [*Schaming and Rotstein*, 1990] or in an intraplate setting [*Coffin and Gahagan*, 1995]. In the following, we will first collate our results with these hypotheses on the origin of the southern Kerguelen Plateau.

Crustal thickness and subdivisions. The total thickness of the igneous crust (i.e., including upper crust, lower crust and the basal reflecting zone) beneath the Raggatt Basin is 20-22 km. This is consistent with a thickened oceanic crust formed above a mantle plume [*White et al.*, 1992] and is approximately 3.5 times the thickness of standard oceanic crust. Crustal structure of thickened oceanic crust formed at a seafloor spreading center is dominated by layer 3 thickening [*Mutter and Mutter*, 1993]. The crustal thickening beneath the Raggatt Basin is dominated by the thickening of the lower crust. The ratio of the thickness of upper crust to lower crust is, on average, 0.35 for the Raggatt Basin crust, whereas it is ~0.60 for a standard oceanic crust [*Mutter and Mutter*, 1993]. If we assume an oceanic origin for the Raggatt

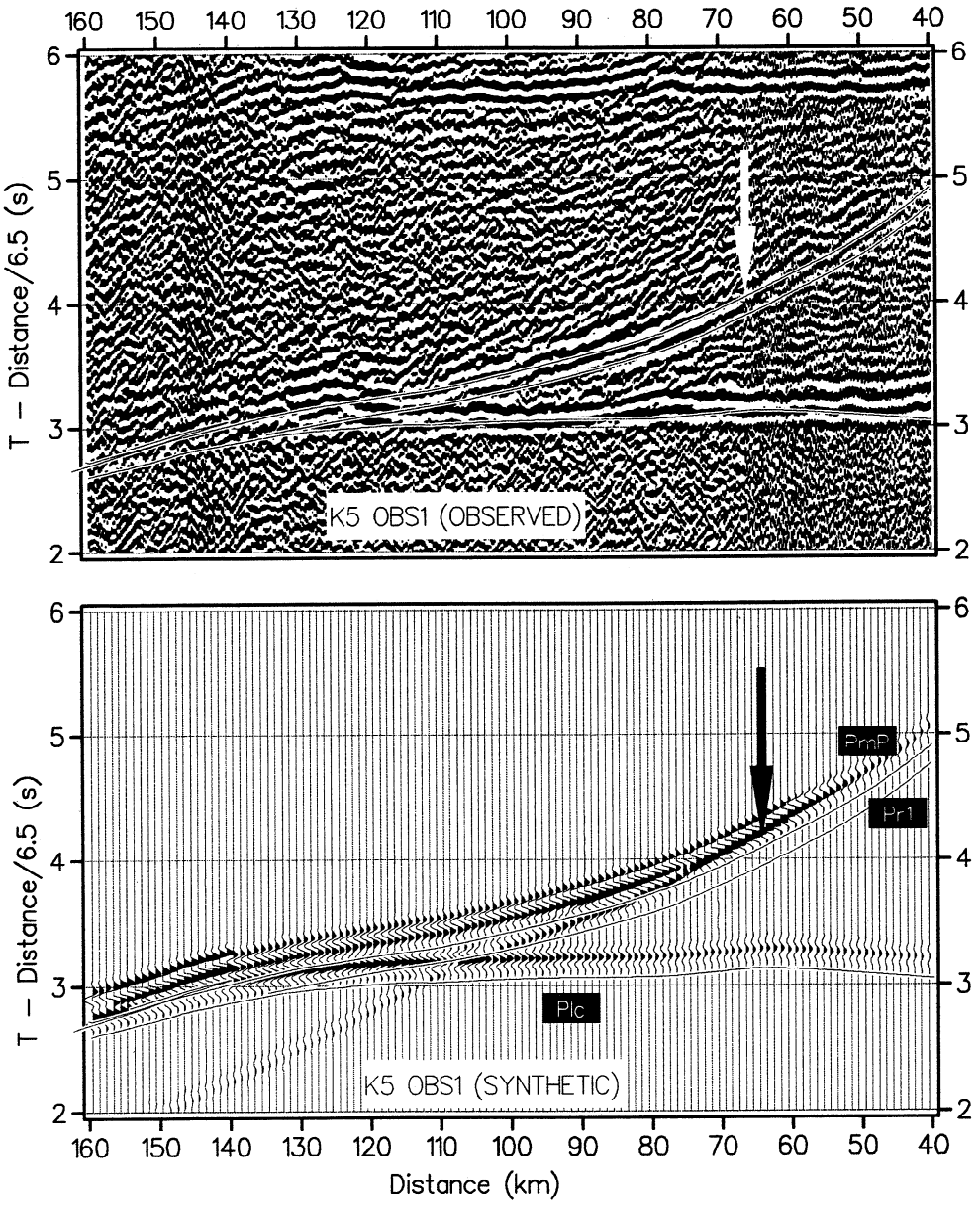

Figure 17. Same as figure 16, but for OBS 1.

Basin, this may indicate an emplacement at an active seafloor spreading center (like Iceland) rather than in an intraplate location (like Hawaii).

Upper crust. Velocities found in the upper crust of the Raggatt Basin are consistent with velocities found in oceanic layer 2, ranging from 2.5 to 6.6 km/s [*White et al.*, 1992], but its thickness is roughly 2.6 times the average thickness of layer 2 in normal oceanic crust. Basalts were drilled in the upper 50 m of the basement in the Raggatt Basin at Site 750 (Figure 2) [*Schlich et al.*, 1989], and multichannel profiles show dipping reflectors in the basement, characteristic of subaerial basaltic flows [*Coffin et al.*, 1990; *Schaming and Rotstein*, 1990].

Seismic velocities in the basement inferred from our data (from 3.80 km/s at the top to 6.50 km/s at the bottom) agree with a basaltic composition for the whole upper crust. The intracrustal reflectors identified in the upper crust can be interpreted in term of a transition between extrusives (metabasalts or pillows lavas) and intrusives (dyke complexes), between porous and nonporous rocks, or as a boundary where hydrothermal circulation stops [*Minshull et al.*, 1991]. Local low-velocity zones in the upper crust, with velocities (poorly constrained by the data) ranging between 5.0 and 6.0 km/s, can be due to alteration, changes in composition between different volcanic flows, or interlayered sediments between basalt flows.

The upper crust–lower crust interface is marked by a velocity discontinuity between 6.00-6.50 km/s (at the bottom of the upper crust) and 6.60-6.65 km/s (at the top of the lower crust) and a sharp decrease of the vertical velocity gradient (from ~0.200 to ~0.025 s^{-1}). This gradient discontinuity is commonly observed in standard oceanic crust, but it is often associated with a gradual transition zone between layer 2 and layer 3. The interface between the upper and lower crust was unambiguously identified on each OBS record section; the upper crust (i.e., the basaltic layer with dipping reflectors) clearly does not extend deeper than 9.80 km, and velocities did not exceed 6.50 km/s at the bottom of the upper crust.

Lower crust. We assume that there is no thermal anomaly in the southern Kerguelen Plateau, and consequently, the average geotherm in the lower crust is 20°C/km. This assumption is reasonable as the southern Kerguelen Plateau is Cretaceous (~110 Ma), no evidence of recent volcanic activity has been recorded in the Raggatt Basin [*Ramsay et al.*, 1986], and kinematic reconstructions suggest that the Kerguelen hot spot is located beneath the northernmost part of the Kerguelen Plateau [*Royer et al.*, 1991]. At 20 km depth (pressure 6 kbar), we can expect a temperature of 400°C. In this pressure-temperature condition, the compressional velocity of a gabbro should be around 7.40 km/s [*Christensen*, 1979], which is significantly higher than the velocity estimated in the Raggatt Basin (6.90 km/s).

If emplacement of the southern Kerguelen Plateau is related to Kerguelen mantle plume, the model of *White and McKenzie* [1989] predicts a thermal anomaly of ~150°C in the mantle to generate a 20-km thick igneous crust [*White and McKenzie*, 1989, Figure 3]. Such a thermal anomaly produces an enrichment in MgO from 11% for normal oceanic crust formed with a mantle potential temperature of 1280°C to 17% with a mantle potential temperature of 1480°C [*McKenzie and Bickle*, 1988]. Resulting magnesian-rich gabbros will have, at a given depth, a higher velocity than gabbros found in normal-thickness oceanic crust [*White and McKenzie*, 1989]. Results of these theoretical calculations agree with the conclusions, based on the compilation of a large set of wide-angle seismic studies of the oceanic crust, showing that seismic velocity in layer 3 increases when the crustal thickness increases [*Mutter and Mutter*, 1993]. This is also in good agreement with the observation of high seismic velocities (> 7.2 km/s) at the base crust of most oceanic plateaus (e.g., Madagascar Ridge [*Sinha et al.*, 1981], Alpha Ridge [*Forsyth et al.*, 1986], Madeira-Tore Rise [*Peirce and Barton*, 1991], northern Kerguelen Plateau [*Charvis et al.*, 1995], and Marquesas Islands [*Caress et al.*, 1995]). The alternative plume head model also generates melt enriched with MgO, with concentration ranging from 16 to 19%. The concentrations are higher for younger oceanic lithosphere and higher excess temperatures in the plume head [*Farnetani and Richards*, 1994]. Oceanic mafic granulites recovered as xenoliths in volcanic rocks of the Tertiary Kerguelen Archipelago are interpreted to represent samples of underplated mafic material located at the base of the crust and characterized by velocities of 7.2-7.5 km/s [*Grégoire et al.*, 1994; *Recq et al.*, 1990]. The lack of high velocities at the base of the crust of Raggatt Basin emphasized by our data set is not consistent with an oceanic origin of the southern Kerguelen Plateau.

Reflective zone and upper mantle. The reflective lower crust (RZ) described beneath the Raggatt Basin is very atypical in oceanic crust settings. The crust-mantle transition in the oceanic crust is known to be constituted by the intercalation of mafic and ultramafic material [e.g., *Christensen and Salisbury*, 1975; *Karson et al.*, 1984]. Nevertheless, the scale of this lamination is often too fine (< 0.3 km) to be detected by the seismic signal we used during the KeOBS experiment (1-km wavelength at lower crustal depths). Furthermore, the average velocities expected for a mafic-ultramafic intercalation (7.30 km/s) is much higher than the velocity estimated in the reflective lower crust of the Raggatt Basin (i.e., 6.70 km/s). The reflective zone is, on average, a low-velocity zone at the base of the crust. In the oceanic domain, low-velocity zones at the base of the crust have sometimes been reported [*Collins et al.*, 1989; *Lewis and Snydsman*, 1979; *Mithal and Mutter*, 1989], but they are usually located at the base of the crust, are less than 10 km deep, and are interpreted as serpentinized peridotites of the upper mantle. This interpretation is not suitable in the case of the Raggatt Basin owing to the depth at which this low-velocity zone is observed (19-25 km).

Comparison with Iceland. The Kerguelen Plateau is often interpreted as the Cretaceous equivalent of Iceland. Iceland results from the interaction of the Mid-Atlantic Ridge with the Iceland hot spot over the past ~16 Myr. Recent seismic studies pointed out a 20- to 24-km-thick crust, with a velocity-depth function consistent with thickened oceanic crust [*Bjarnason et al.*, 1993].

Although Iceland is an active structure with a high geothermal gradient, its velocity-depth function can be compared with that determined beneath the southern Kerguelen Plateau, as it is sufficiently cold to consist of unmelted rocks [*Bjarnason et al.*, 1993]. Nevertheless, the high geothermal gradient in the Icelandic crust probably leads, at a given depth and for a similar composition, to lower seismic velocities than in the Kerguelen Plateau crust.

The crustal velocity-depth function down to 20 km depth in the Raggatt Basin is comparable with that of Iceland (Figure 18); the whole crustal thickness, as well as thicknesses of layers 2 and 3, are similar. Nevertheless, the velocity at 15 km depth (maximum depth at which velocities are well constrained) beneath Iceland is often higher than the velocity beneath Raggatt Basin and reaches ~7.2 km/s at the base of the Icelandic crust. Higher velocities in the lower crust of Iceland compared with Raggatt Basin, despite the very high geothermal gradient beneath Iceland, suggest that these two features cannot share a similar origin.

Comparison with northern Kerguelen Plateau and Enderby Basin. Velocities in the lower crust of the Raggatt Basin are significantly lower than those of surrounding oceanic areas (Figure 18). On the basis of kinematic reconstructions, formation of the Enderby Basin is assumed to have been synchronous with the formation of the Perth and Cuvier Basins (anomalies M0 to M10, west of Australia) and with the emplacement of the Kerguelen Plateau, although no magnetic anomalies in the Enderby Basin confirmed this interpretation [*Royer and Sandwell*, 1989]. The crust of the Enderby Basin is

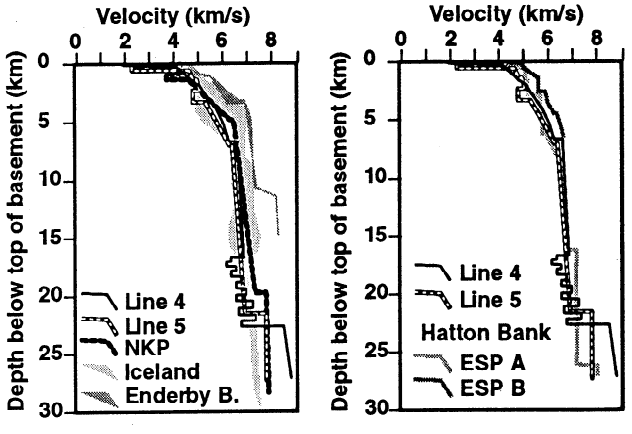

Figure 18. Comparison of our average velocity function in the Raggatt Basin (left) with the envelope of velocity depth functions across Iceland [*Bjarnason et al.*, 1993], with the average velocity function in the northern Kerguelen Plateau (NKP) [*Charvis et al.*, 1995], with the average velocity function in the Enderby oceanic Basin [*Operto*, 1995], and (right) with expanded spread profiles (ESP) A and B shot along the Hatton Bank [*Fowler et al.*, 1989; *Morgan et al.*, 1989; *Spence et al.*, 1989].

10-13 km thick and thins gently away from the plateau [*Operto*, 1995]. It is slightly thicker than the standard oceanic crust (7.08 ± 0.78) but is similar to the mean thickness of the oceanic crust surrounding the Iceland mantle plume, 10.3 ± 1.7 km [*White et al.*, 1992]. Velocities in layer 3 are 6.90-7.00 km/s at the top (at ~8 km depth) and 7.40-7.50 km/s at the base of the crust (at ~16 km depth). The high velocities, higher than in a normal oceanic crust, agree with olivine-rich gabbros and corroborate, as well as the thickening of the crust, a hot spot influence during the formation of oceanic crust [*Operto*, 1995; *Operto et al.*, 1994]. The velocities reached at a given depth in the Enderby Basin are significantly greater than in the Raggatt Basin (Figure 18), and the expected positive correlation between crustal thickness and average velocity in layer 3 [*Mutter and Mutter*, 1993] is clearly not observed.

Igneous crust beneath the northern Kerguelen Plateau consists of three layers, with a total thickness ranging from 19 to 21 km. The upper one, 1.2-2.3 km thick with velocities ranging from 3.8 to 4.9 km/s, could be either composed of low-density lava flows or volcanic material interlayered with sediments [*Munschy and Schlich*, 1987; *Charvis et al.*, 1993, 1995]. The second layer is 2.3-3.3 km thick and has velocities ranging downward from 4.7 to 6.7 km/s. Velocities and thicknesses are comparable in these two layers to those observed in the upper crust of the Raggatt Basin, but the transition to the lower crust is gradual in the northern Kerguelen Plateau [*Charvis et al.*, 1995; *Operto*, 1995], whereas it is a sharp, first-order discontinuity beneath the Raggatt Basin. In the lower crust of the northern Kerguelen Plateau, velocities increase from 6.60 km/s at ~8.0 km depth (near the top of the layer) to 7.40 km/s at the base of the crust. The value reached at the base of the crust, which agrees with the model of *White and McKenzie* [1989], is significantly higher that the one observed in the Raggatt Basin (Figure 18).

Reflections from the base of the crust as well as the strong and long wave train *PmP* described in the Raggatt Basin contrast with the seismic transparency of the lowermost crust and Moho in the northern Kerguelen Plateau and a more simple seismic pattern in the oceanic Enderby Basin [*Charvis et al.*, 1995; *Operto*, 1995]. In the northern domain, the base of the crust is seismically transparent (that is, no internal reflections are observed on the record sections), and the lower crust extends down to Moho without a reflective transition zone between the base of the lower crust and the Moho. In addition, weak *PmP* and the lack of *Pn* (except on one OBS record section) suggest that the Moho is a gradual transition zone and a shallow velocity gradient in the upper mantle [*Charvis et al.*, 1995; *Operto*, 1995]. In the Enderby Basin, data show the classical simple pattern observed in the oceanic crust, including the refraction in the layer 3, a sharp reflection from Moho, and a refraction in the upper mantle, but do not show evidence of a reflective lower crust at the base of the crust.

Is the Southern Kerguelen Plateau a Volcanic Passive Margin?

The emplacement of the Cretaceous Kerguelen Plateau (including Broken Ridge) was nearly complete at ~110 Ma in the nascent Indian Ocean [*Leclaire et al.*, 1987; *Royer and Coffin*, 1992; *Whitechurch et al.*, 1992]. The southern Kerguelen Plateau area is presently separated from the Antarctic continental margin (approximately 500 km southward) by the Princess Elisabeth Trough. During the rifting between India and Antarctica (~130 Ma [*Royer and Coffin*, 1992]), continental fragments may have been detached and isolated for the main continental masses by a jump of the rifting zone. Thus the alternative hypothesis for the origin of the Raggatt Basin is that it consists of a fragment of continental crust.

Upper crust. Velocities we computed in the upper crust are consistent with those observed in oceanic layer 2, and we know from previous studies that the basement of the southern Kerguelen Plateau is basaltic. Nevertheless, within the lower part of the upper crust, velocities are also consistent with those found in the upper continental crust (5.95±0.73 km/s at 5 km depth) [*Christensen and Mooney*, 1995]. Furthermore, along volcanic passive margins, the limit between the basaltic layer (characterized by dipping reflectors) and the upper continental crust is not underlined by a sharp velocity contrast [e.g., *Mutter et al.*, 1984; *Spence et al.*, 1989]. Thus, a thin upper continental crust cannot be precluded from seismic structure beneath the Raggatt Basin.

Lower crust. Velocities within the lower crust of Raggatt Basin and the average velocity in the RZ are consistent with the range of velocities observed in the lower continental crust. The histogram of velocities found in the lower continental crust located in rift zones shows a maximum for velocities of ~6.70 km/s, and velocities between 6.90 and 7.10 km/s are commonly observed at the base of the rifted continental crust [*Christensen and Fountain*, 1975; *Christensen and Mooney*, 1995; *Holbrook et al.*, 1992].

Reflective zone and upper mantle. The reflectivity at the base of the crust and the azimuthal anisotropy at the base of the crust and in the upper mantle may be the result of extension of the continental crust. The reflectivity of the lower crust has been extensively imaged using wide-angle seismic data in continental areas affected by extension and/or magmatism. Two main causes are classically invoked to explain the reflectivity of the lower continental crust [*Holbrook et al.*, 1991]: (1) mafic intrusions or igneous cumulate layering in relation to magmatism, and (2) ductile strain fabrics in relation to extension.

We believe that these two mechanisms could play a role in the reflectivity at the base of the crust of the Raggatt Basin. Nevertheless, ductile shearing is probably the mechanism which dominates. This would explain the low average velocity in the RZ as well as the anisotropy in the RZ (magmatic intrusions alone would not generate anisotropy in the RZ).

The low reflection coefficients pointed out in the upper part of the RZ (0.030-0.056), as well as the velocities, are consistent with ductile shear zones into a mafic, homogeneous, lower crust [*Holbrook et al.*, 1991], and velocities (between 6.20 and 6.60 km/s in the low velocity layers and between 6.40 and 7.00 km/s in the high velocity layers) are consistent with mafic mylonites [*Jones and Nur*, 1982]. These structures would have resulted from the extension of the crust.

The lower part of the reflective zone is characterized by higher reflection coefficients (0.080) and velocities ranging from 6.70 to 6.80 km/s in the low velocity layers and from 7.30 to 7.40 km/s in the high velocity layers. *Holbrook et al.* [1991] estimated reflection coefficients of 0.04-0.06 for mafic intrusions into the mafic lower crust, but note that these values can be doubled by constructive interference. The higher reflection coefficients, as well as the velocities in the high-velocity layers, are consistent with mafic rocks intruding surrounding country rock.

Ductile shearing favors seismic azimuthal anisotropy at different scales. In the Basin and Range, anisotropy results from elongated ductile shears in the direction of the extension [*Carbonell and Smithson*, 1991]. In the Raggatt Basin, internal

reflections from the reflective zone are only observed in the NNW-SSE direction, and this might indicate a large-scale anisotropy related to extension of continental crust approximately in this direction. Magmatic intrusion contributions, which affects the structure in a similar way in the two directions, may be too weak to affect significantly the wave field recorded along line 5 (although some events can be observed for OBS 3 and 2 along line 5; see Figures 11c and 11d). The lower average velocity determined in the reflective zone in the NNW-SSE direction compared to that in the E-W direction might be related to underestimation of the seismic velocity along line 4 in relation to an apparent, more heterogeneous RZ. Thus azimuthal anisotropy in the reflective lower crust has probably a tectonic origin and is consistent with the extension of the crust in the NNW-SSE direction.

The 8% anisotropy in the upper mantle, with the fast direction in the NNW-SSE direction, is also consistent with the NW-SE direction of extension inferred from anisotropy in the reflective zone. Indeed, anisotropy in the upper mantle is usually interpreted to result from preferential alignment of olivine crystals in the direction of extension [*Christensen and Salisbury*, 1979].

Reflectivity across continental margins is known to be well developed beneath moderately stretched continental shelves and to decrease toward the ocean-continent transition [*Hutchinson et al.*, 1992]. So the decrease of the reflectivity of the lowermost crust, from south to north, suggested along the NNW-SSE line 4 is consistent with the southern Kerguelen Plateau being a fragment of the Antarctic continental margin.

Interpretative Model

The thickness of the possibly continental crust beneath the Raggatt Basin, excluding the sediments and the basaltic part of the upper crust, varies between 15-17 km and ~20 km, depending on whether we consider that the whole upper crust is basaltic or not. This fragment mostly consists of lower continental crust, as the upper continental crust is very thin or absent. We believe that a model of extension based on differential stretching between the upper and lower crust may explain the seismic structure of the Raggatt Basin (Figure 19). This model was used to explain the structure of the Basin and Range- Colorado Plateau transition [*McCarthy and Parsons*, 1994] and the structure of the Rockall Trough [*Hauser et al.*, 1995]. The model of extension involves simple shear deformation in the upper crust along low-angle faults and pure shear deformation in the lower crust [*McCarthy and Parsons*, 1994]. Denudation of the lower crust, resulting in the simple shear deformation, would explain that the upper crust

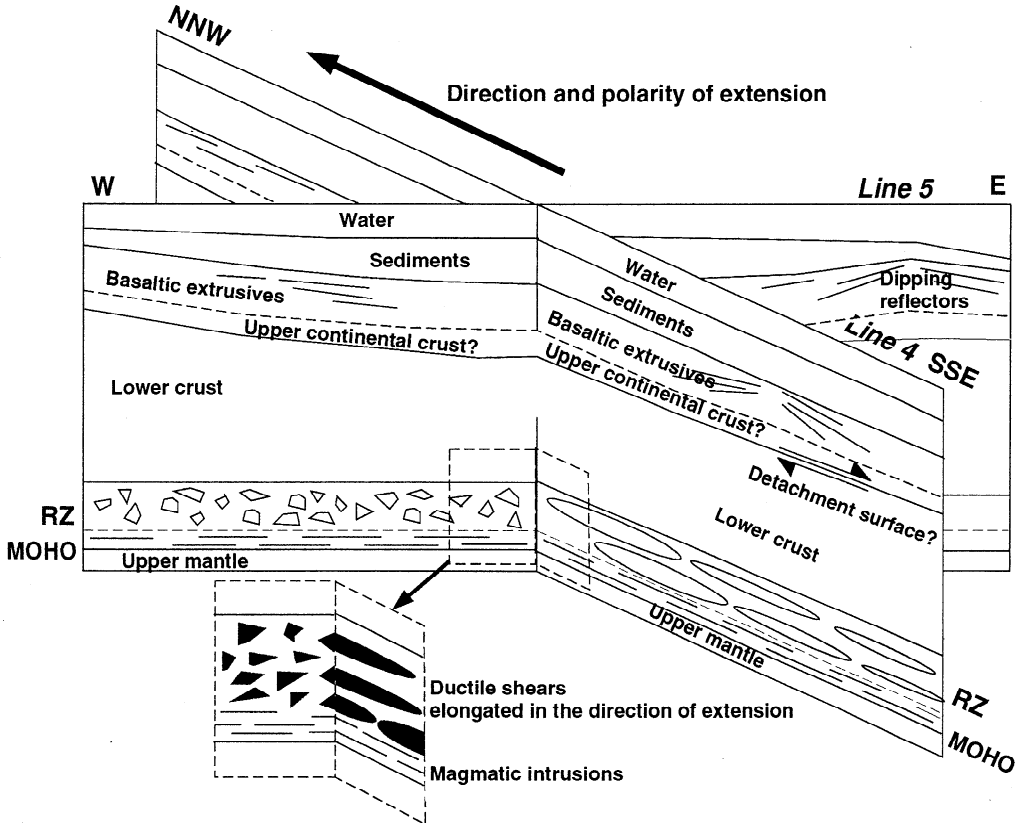

Figure 19. Schematic interpretative model of formation of Raggatt Basin (not to scale). Continental crust overlain by basalt flows is stretched in the NNW-SSE direction. Basalt extrusives represent widespread flood basalts in relation to the Kerguelen mantle plume. Thin upper continental crust may be present below basalts even if this boundary is seismically transparent. Extension caused decoupling between the upper crust and the lower crust along a primary rheological (brittle/ductile) detachment surface (indicated by arrows along the upper crust-lower crust interface). Simple shear in the brittle upper crust caused its severe thinning as pure shear mechanism maintained the lower crust thickness across the whole basin. Top of the reflective lower crust (RZ) is composed of ductile shears elongated in the direction of extension. The scale of these features increases from south to north in relation to the amount of extension. Magmatic intrusions are confined to the base of the reflective lower crust.

is absent or very thin. On the contrary, a pure shear deformation would explain that the lower crust is still thick in relation to a small extension and its thickness remains almost constant over a broad distance. Moderate extension would also explains that the RZ (i.e., the reflectivity in connection with ductile shearing) is confined at deep levels between 19 and 23-24 km depth. With such a mechanism, *McCarthy and Parsons* [1994] note that the top of the lower crust in the Basin and Range, once at 20 km depth, was elevated to ~11 km depth which is approximately the depth of the upper crust-lower crust interface in the Raggatt Basin.

In the plume-related large igneous provinces (e.g., northern North Atlantic Volcanic Province), extrusive basalts extended on the adjacent continents without associated contiguous underplating [*White and McKenzie*, 1989]. The extrusive basalts on top of the crust of Raggatt Basin may be the result of a similar widespread basaltic volcanism extended away from the central plume. Contiguous underplating is confined over a much more narrow area along the margin (e.g., 70 km perpendicularly to the margin in the North Atlantic [*Fowler et al.*, 1989]) in relation to the rapid thinning of the crust as the plume head impinges at the base of the lithosphere. Obviously, it is not possible from our data to locate the continent-ocean boundary.

The mantle plume-lithosphere rifting model of *White and McKenzie* [1989] postulates that volcanism may spread across a 2000-km-wide area in relation to abnormally hot asthenosphere. This agrees with the fact that the Kerguelen hot spot was probably responsible for the formation of a much larger igneous province than the Kerguelen Plateau alone, beginning at 120-130 Ma with the eruption of the Naturalist Plateau and Bunbury basalts west of Australia. The Rajmahal Trapps along the northeastern margin of India erupted at ~117 Ma, while lamprophyres of Prince Charles Mountains were emplaced at ~110 Ma near the Antarctic continental margin [*Davies et al.*, 1989; *Mahoney et al.*, 1995; *Storey et al.*, 1992].

The direction of extension (NNW-SSE) inferred from the anisotropy in the reflective lower crust and in the upper mantle is consistent with the direction of seafloor spreading between Indian and Australian-Antarctic plates at ~110 Ma [*Royer and Sandwell*, 1989]. In addition, the polarity of the extension from south to north, inferred from the variability of the reflectivity in the NNW-SSE direction, agrees with the oceanic origin of the northern Kerguelen Plateau [*Charvis et al.*, 1993, 1995; *Operto*, 1995] and suggests that the southern Kerguelen Plateau might represent a fragment of the Australian-Antarctic margin (Figure 19).

Comparison Between the Kerguelen Volcanic Province and the North Atlantic Volcanic Province

On the basis of deep structure and relative location of main geological features, we compare a south-north profile across the Kerguelen Cretaceous Volcanic Province with an east-west profile across the North Atlantic Volcanic Province. From the continent toward the hot spot we observed : (1) the continental margin (Antarctic and Irish margins) affected by volcanic activity contemporaneous with the rifting phase, (2) a 200-300 km wide, 2500-3500 m deep trough separating the margin from a submarine plateau (Princess Elisabeth and Rockall troughs), (3) a continental plateau overlain by basaltic flows (southern Kerguelen Plateau and Rockall Plateau), (4) the main volcanic plateau associated with the activity of the hot spot (northern Kerguelen Plateau and Iceland), and (5) the neighboring oceanic basin only slightly affected by the vicinity of the hot spot (Enderby Basin or Iceland Basin).

The ~400-km-wide Rockall plateau is covered by widespread extrusive basaltic volcanism in relation to the Iceland mantle plume [*White and McKenzie*, 1989]. Contiguous underplating is confined into a narrow area along the margin and is absent beneath most of the Rockall plateau [*Fowler et al.*, 1989; *Morgan et al.*, 1989]. Crustal thickness (~22 km) and velocities in the lower crust ranging from 6.6 at 9 km depth to 7.1 km/s at the base of the crust are similar to those determined beneath the Raggatt Basin (Figure 18).

Cinematic, Geochemical, and Geological Arguments

Poor constraints on the opening of the Indian Ocean when the plateau formed are partly due to the lack of datable magnetic anomalies in the Enderby Basin, the scarcity of basement samples, the various geochemical anomalies described [*Mahoney et al.*, 1995; *Storey et al.*, 1992], and the lack of deep seismic sounding. This allows many speculative hypotheses for the plateau's emplacement. Hypotheses range from long-lived hot-spot tracks [*Müller et al.*, 1993], to catastrophic volcanic phase associated with the incipient activity of the Kerguelen Plume [*Coffin and Eldholm*, 1994; *Coffin and Gahagan*, 1995] in a purely oceanic area or with the possible implication of continental fragments [*Operto and Charvis*, 1995; *Ramsay et al.*, 1986].

The argument that the Kerguelen Plateau is a rifted subsided continental lithosphere [*Dietz and Holden*, 1970; *Schlich et al.*, 1971] is not supported by most of the plate reconstructions which place the east side of India against Antarctica and which provide a reasonable predrift fit of the continents without the need to incorporate the plateau [*Norton and Sclater*, 1979; *Powell et al.*, 1988]. Nevertheless, owing to the poor constraints on the reconstructions and the fact that the extension of continental lithosphere along margins is not taken into account for most reconstructions, we believe that cinematic reconstruction cannot preclude the presence of a continental fragment beneath the southern Kerguelen Plateau.

The type of emplacement of the Cretaceous Kerguelen Plateau, supported by trace element and isotope geochemistry, is that the plateau resulted from excess volcanism linked to a mantle plume in an extensional or spreading zone in a scheme similar to present-day Iceland [*Storey et al.*, 1989, 1992]. Isotopic compositions of most Kerguelen Plateau basalts suggest that they have the same source as the hot spot basalts from Kerguelen and Heard Islands.

Nevertheless, low $^{206}Pb/^{208}Pb$ ratios and high La/Nb ratios suggest that the source of the Kerguelen Plateau basalts was contaminated by the Gondwana continental lithosphere [*Storey et al.*, 1992]. An extreme expression of this signature is outlined by tholeiitic basalts recovered at Site 738 on the southernmost part of the Kerguelen Plateau (Figure 2). These lavas show anomalous Sr, Nd, and Pb isotopic composition compared with other lava of the Kerguelen Archipelago and the Kerguelen Plateau, suggesting that they originate from the Gondwana subcontinental lithosphere and that possibly they were contaminated by an overlying continental crust, although this latter hypothesis is difficult to ascertain from geochemical analyses [*Alibert*, 1991]. Furthermore, the estimated degree of melting for the Kerguelen Plateau basalts is similar (or even less) than required for mid-ocean ridge basalt genesis [*Salters et al.*, 1992]. This appears to exclude thickening of the igneous crust by an increased degree of melting in the mantle [*Salters et al.*, 1992].

Conclusions

The detailed modeling of two wide-angle seismic lines shot in the Raggatt Basin, on top of the southern Kerguelen Plateau, led to the following conclusions concerning the deep structure and the origin of this part of the plateau.

1. the crust beneath the Raggatt Basin is 22-23 km thick. It consists of (1) a 5.3 km thick upper crust (velocities from 3.80-4.50 km/s at top to 6.00-6.50 km/s at bottom); (2) a 9- to 10-km thick lower crust with velocities increasing linearly with depth from 6.63 km/s at 9 km depth to 6.90 km/s at 19 km depth; (3) in the NNW-SSE direction, a reflective lower crust observed between 19 km down to Moho. The reflective lower crust is modeled as interlayered high- and low-velocity layers with an average velocity of 6.70 km/s, and it is not identifiable in the perpendicular direction, where average velocity above Moho reaches at least 6.90 km/s. Velocity at the top of upper mantle is 8.6 km/s in the NNW-SSE direction and 8.0 km/s in the perpendicular direction leading to a 8% anisotropy.

2. The crust of Raggatt Basin is interpreted as a stretched continental crust overlain by extrusive basalts. The upper crust may be composed either of extrusive basalts down to the top of lower crust or of a thin upper continental crust overlain with extrusive basalts. The reflectivity and the anisotropy of the lower crust are interpreted as the result of extension (i.e., related to ductile shears elongated in the direction of extension). Magmatic intrusions could be confined to the base of the reflective lower crust.

3. The very low thickness ratio between upper and lower continental crust is interpreted as related to differential stretching between the upper crust and the lower crust. Simple shear deformation of the upper crust caused its severe thinning and possible denudation of lower crust, while pure shear deformation allowed a thick lower crust over the whole basin. Extrusive basalts are interpreted as flood basalts extruded onshore from the central Kerguelen mantle plume.

4. The Cretaceous Kerguelen Volcanic Province can be compared to the North Atlantic Large Igneous Province. The deep structure of Raggatt Basin is consistent with that of the continental Rockall Basin, and the structure of the northern Kerguelen Plateau is similar to that of Iceland.

These results are consistent with isotopic studies of the basaltic basement and with samples of continental rocks dredged on the top of the southern Kerguelen Plateau and in the Labuan Basin, if they are not ice rafted. Unfortunately, relation of the southern Kerguelen Plateau to the Antarctic margin, to the Naturaliste Plateau, and to the Australian margin are unknown, mainly owing to the scarce data.

Acknowledgments. We thank Yann Hello (ORSTOM) for operating the OBSs at sea, Yvon Fercoq (CGM) and the crew of M/V Marion Dufresne, Bernard Ollivier (TAAF), the IFREMER-GENAVIR party (Jean Le Pavec, Philippe Le Doze, and Jean-Luc Le Philippe), and colleagues of the MD66/KeOBS scientific party. We acknowledge Mike Coffin for his useful comments and help in editing the manuscript, Colin Zelt for providing us with his ray tracing and inversion programs, and Francois Glangeaud (CEPHAG) for his help in processing the data. One of us (P.C.) also thanks Roland Schlich (EOPGS) and Mike Coffin (UTIG) for making their database on the Kerguelen Plateau available during the preparation of the cruise and interpretation of the data. We are grateful to D.R. Hutchinson, I.D. Reid, and an anonymous reviewer. The MD66/KeOBS cruise was financially and technically supported by Terres Australes et Antarctiques Françaises (TAAF, then Mission de Recherche) and Institut Français de Recherche Scientifique pour le Développement en Coopération (ORSTOM, UR 14). UMR Géosciences Azur, EP125 contribution 23.

References

Alibert, C., Mineralogy and geochemistry of a basalt from site 738: Implications for the tectonic history of the southernmost part of the Kerguelen Plateau, *Proc. Ocean Drill. Program, Sci. Results, 119,* 293-298, 1991.

Angoulvant-Coulon, M.-P., and R. Schlich, Mise en évidence d'une nouvelle direction tectonique sur le plateau de Kerguelen, *C. R. Acad. Sci., Ser. II, 319* (2), 929-935, 1994.

Bjarnason, I.T., W. Menke, O.G. Flovenz, and D. Caress, Tomographic image of the mid-Atlantic plate boundary in southwestern Iceland, *J. Geophys. Res., 98* (B4), 6607-6622, 1993.

Carbonell, R., and S.B. Smithson, Large-scale anisotropy within the crust in the Basin and Range province, *Geology, 19,* 698-701, 1991.

Caress, D.W., M.K. McNutt, R.S. Detrick, and J.C. Mutter, Seismic imaging of hotspot-related crustal underplating beneath the Marquesas Islands, *Nature, 373,* 600-603, 1995.

Charvis, P., S. Operto, L.K. Konnecke, M. Recq, Y. Hello, F. Houdry, P. Lebellegard, R. Louat, and F. Sage, Structure profonde du domaine nord du plateau de Kerguelen (océan Indien austral): Résultats préliminaires de la campagne MD66/KeOBS, *C. R. Acad. Sci., Ser. II, 316,* 341-347, 1993.

Charvis, P., M. Recq, S. Operto, and D. Bréfort, Deep structure of the northern Kerguelen-Plateau and hot spot-related activity, *Geophys. J. Int., 122* (3), 899-924, 1995.

Christensen, N.I., Compressional wave velocities in rocks at high temperatures and pressures, critical thermal gradients, and crustal low-velocity zones, *J. Geophys. Res., 84* (B12), 6849-6857, 1979.

Christensen, N.I., and D.M. Fountain, Constitution of the lower continental crust based on experimental studies of seismic velocities in granulite, *Geol. Soc. Am. Bull., 86,* 227-236, 1975.

Christensen, N.I., and W.D. Mooney, Seismic velocity structure and composition of the continental crust: A global view, *J. Geophys. Res., 100* (B7), 9761-9788, 1995.

Christensen, N.I., and M.H. Salisbury, Structure and constitution of the lower oceanic crust., *Rev. Geophys. Space Phys., 13* (1), 57-86, 1975.

Christensen, N.I., and M.H. Salisbury, Seismic anisotropy in the oceanic upper mantle: Evidence from the Bay of Islands ophiolite complex, *J. Geophys. Res., 84* (B9), 4601-4610, 1979.

Coffin, M.F., H.L. Davies, and W.F. Haxby, Structure of the Kerguelen Plateau province from Seasat altimetry and seismic reflection data, *Nature, 324,* 134-136, 1986.

Coffin, M.F., and O. Eldholm, Large igneous provinces: Crustal structure, dimensions, and external consequences, *Rev. Geophys., 32* (1), 1-36, 1994.

Coffin, M.F., and L.M. Gahagan, Ontong Java and Kerguelen Plateaux: Cretaceous Icelands?, *J. Geol. Soc. London, 152,* 1047-1052, 1995.

Coffin, M.F., M. Munschy, J.B. Colwell, R. Schlich, H.L. Davies, and Z.-G. Li, Seismic stratigraphy of the Raggatt Basin, southern Kerguelen Plateau: Tectonic and paleoceanographic implications, *Geol. Soc. Am. Bull., 102,* 563-579, 1990.

Collins, J.A., G.M. Purdy, and T.M. Brocher, Seismic velocity structure at Deep Sea Drilling Project Site 504B, Panama Basin: Evidence for thin oceanic crust, *J. Geophys. Res., 94,* 9283-9302, 1989.

Davies, H.L., S.-S. Sun, F.A. Frey, I. Gautier, M.T. McCulloch, R.C. Price, Y. Bassias, C.T. Klootwijk, and L. Leclaire, Basalt basement from the Kerguelen Plateau and the trail of a Dupal plume, *Contrib. Mineral. Petrol., 103,* 457-469, 1989.

Deichmann, N., and J. Ansorge, Evidence for lamination in the lower continental crust beneath the Black Forest (southwestern Germany), *J. Geophys., 52,* 109-118, 1983.

Dietz, R.S., and J.C. Holden, Reconstruction of Pangea: Breakup and dispersion of continents, Permian to Present, *J. Geophys. Res., 75,* 4939-4956, 1970.

Farnetani, C., and M.A. Richards, Numerical investigations of the mantle plume initiation model for flood basalt events, *J. Geophys. Res., 99* (B7), 13813-13833, 1994.

Forsyth, D.A., I. Asudeth, A.G. Green, and H.R. Jackson, Crustal structure of the northern Alpha ridge, *Nature, 322,* 349-352, 1986.

Fowler, S.R., R.S. White, G.D. Spence, and G.K. Westbrook, The Hatton Bank continental margin, II, Deep structure from two-ship expanding spread seismic profiles, *Geophys. J., 96,* 295-309, 1989.

Fritsch, B., Tectonique extensive et mouvements verticaux du plateau de Kerguelen (océan Indien), Thèse d'université, Université Louis Pasteur, Ecole et Obs. de Phys. du Globe, Strasbourg, France, 1992.

Fritsch, B., R. Schlich, M. Munschy, F. Fezga, and M.F. Coffin, Evolution of the Southern Kerguelen Plateau deduced from seismic stratigraphic studies and drilling at sites 748 and 750, *Proc. Ocean Drill. Program, Sci. Results, 120,* 895-906, 1992.

Fuchs, K., and G. Müller, Computation of synthetic seismograms with the reflectivity method and comparison with observations, *Geophys. J. R. Astron. Soc., 23,* 417-433, 1971.

Grégoire, M., N. Mattielli, C. Nicollet, J.Y. Cottin, H. Leyrit, D. Weis, N. Shimizu, and A. Giret, Oceanic mafic granulite xenoliths from the Kerguelen Archipelago, *Nature, 367,* 360-363, 1994.

Hauser, F., B. O'Reilly, M., A. Jacob, W., Brian, P. Shannon, M., J. Makris, and U. Vogt, The crustal structure of the Rockall Trough: Differential stretching without underplating, *J. Geophys. Res., 100* (B3), 4097-4116, 1995.

Holbrook, W.S., R.D. Catchings, and C.M. Jarchow, Origin of deep crustal reflections: Implications of coincident seismic refraction and reflection data in Nevada, *Geology, 19,* 175-179, 1991.

Holbrook, W.S., W.D. Mooney, and N.I. Christensen, The seismic velocity structure of the deep continental crust in *Continental Lower Crust,* edited by D. M. Foutain, R. Arculus, and R.W. Kay, 1-34 pp., Elsevier Sc., New York, 1992.

Houtz, R.E., D.E. Hayes, and R.G. Markl, Kerguelen Plateau bathymetry, sediment distribution and crustal structure, *Mar. Geol., 25,* 95-130, 1977.

Hutchinson, D.R., M.W. Lee, J. Behrendt, W.F. Cannon, and A.G. Green, Variations in the reflectivity of the Moho Transition Zone beneath the midcontinent rift system of North America: Results from true amplitude analysis of GLIMPCE data, *J. Geophys. Res., 97* (B4), 4721-4737, 1992.

Jones, T.D., and A. Nur, Seismic velocity and anisotropy in mylonites and the reflectivity of deep crustal fault zones, *Geology, 10,* 260-263, 1982.

Karson, J.A., J.A. Collins, and J.F. Casey, Geologic and seismic velocity structure of the crust/mantle in the bay of Islands ophiolite complex, *J. Geophys. Res., 89* (B7), 6126-6138, 1984.

Könnecke, L.K., and M.F. Coffin, Tectonic constraints on the early development of the Kerguelen Plateau, southern Indian Ocean (abstract), *Ann. Geophys.,* 13, part I, C 131, 1995.

Larson, R.L., Geological consequences of superplumes, *Geology, 19,* 963-966, 1991.

Leclaire, L., Y. Bassias, M. Denis-Clocchiatti, H. Davies, I. Gautier, B. Gensous, P.-J. Giannesini, P. Patriat, J. Segoufin, M. Tesson, and J. Wannesson, Lower Cretaceous Basalt and Sediments from the Kerguelen Plateau, *Geo Mar. Lett., 7,* 169-176, 1987.

Levander, A.R., and K. Holliger, Small-scale heterogeneity and large-scale velocity structure of the continental crust, *J. Geophys. Res., 97* (B6), 8797-8804, 1992.

Lewis, B.T.R., and W.E. Snydsman, Fine structure of the lower oceanic crust on the Cocos Plate, *Tectonophysics, 55* (1/2), 87-105, 1979.

Mahoney, J.J., W.B. Jones, F.A. Frey, V.J.M. Salters, D.G. Pyle, and H.L. Davies, Geochemical characteristics of lavas from Broken Ridge, the Naturaliste Plateau and southernmost Kerguelen Plateau: Cretaceous plateau volcanism in the southeast Indian Ocean, *Chem. Geol., 120,* 315-345, 1995.

Mari, J.L., and F. Glangeaud, Spectral matrix filtering applied to VSP processing, *Rev. Inst. Fr. Pétr., 45* (3), 418-434, 1990.

McCarthy, J., and T. Parsons, Insights into the kinematic Cenozoic evolution of the Basin and Range-Colorado Plateau transition from coincident seismic refraction and reflection data, *Geol. Soc. Am. Bull., 106,* 747-759, 1994.

McKenzie, D., and M.J. Bickle, The volume and composition of melt generated by extension of lithosphere, *J. Petrol., 29* (3), 625-679, 1988.

Minshull, T.A., R.S. White, J.C. Mutter, P. Buhl, R.S. Detrick, C.A. Williams, and E. Morris, Crustal structure at the Blake Spur Fracture Zone from expanding spread profiles, *J. Geophys. Res., 96* (B6), 9955-9984, 1991.

Mithal, R., and J.C. Mutter, A low-velocity zone within the layer 3 region of 118 Myr old oceanic crust in the western North Atlantic, *Geophys. J. Int., 97,* 275-294, 1989.

Montigny, R., A.-M. Karpoff, and C. Hofmann, Résultats d'un dragage par 55°18'S-83°04'E dans le Bassin de Labuan (campagne MD 67, océan Indien méridional): Implications géodynamiques (abstract), *Mém. Soc. Géol. de Fr.,* 83, 1993.

Morgan, J.V., P.J. Barton, and R.S. White, The Hatton Bank continental margin, III, Structure from wide angle OBS and multichannel seismic refraction profiles, *Geophys. J. Int., 98* (2), 367-384, 1989.

Müller, R.D., J.-Y. Royer, and L.A. Lawver, Revised plate motions relative to the hotspots from combined Atlantic and Indian Ocean hotspot tracks, *Geology, 21,* 275-278, 1993.

Munschy, M., J. Dyment, M.O. Boulanger, D. Boulanger, J.D. Tissot, R. Schlich, Y. Rotstein, and M.F. Coffin, Breakup and seafloor spreading between the Kerguelen Plateau-Labuan Basin and the Broken Ridge-Diamantina Zone, *Proc. Ocean Drill. Program, Sci. Results, 120,* 931-944, 1992.

Munschy, M., Y. Rotstein, R. Schlich, and M.F. Coffin, Structure and tectonic setting of the 77° E and 75° E grabens, Kerguelen Plateau, South Indian Ocean, *J. Geophys. Res., 98* (B4), 6367-6382, 1993.

Munschy, M., and R. Schlich, Structure and evolution of the Kerguelen-Heard plateau (Indian Ocean) deduced from seismic stratigraphy studies, *Mar. Geol., 76,* 131-152, 1987.

Mutter, C.Z., and J.C. Mutter, Variations in thickness of layer 3 dominate oceanic crustal structure, *Earth Planet. Sci. Lett., 117,* 295-317, 1993.

Mutter, J.C., M. Talwani, and P.L. Stoffa, Evidence for a thick oceanic crust adjacent to the Norwegian Margin, *J. Geophys. Res., 89* (B1), 483-502, 1984.

Nakamura, Y., P.L. Donoho, P.H. Roper, and P. McPherson, Large-offset seismic surveying ocean-bottom seismographs and air guns: Instrumentation and field technique, *Geophysics, 52* (12), 1601-1611, 1987.

National Geophysical Data Center, ETOPO-5 bathymetry/topography data, Natl. Oceanic and Atmos. Admin., Boulder, Colo., 1988.

Norton, I.O., and J.G. Sclater, A model for the evolution of the Indian Ocean and the breakup of Gondwanaland, *J. Geophys. Res., 84,* 6803-6830, 1979.

Ojo, S.B., and R.F. Mereu, The effect of random velocity functions on the travel times and amplitudes of seismic waves, *Geophys. J. R. Astron. Soc., 84,* 607-618, 1986.

Operto, S., Structure et origine du plateau de Kerguelen (océan Indien austral): Implications géodynamiques. Modélisation de données sismiques grand-angle marines, Thése d'université, Université Pierre et Marie Curie, Paris, 1995.

Operto, S., and P. Charvis, Kerguelen Plateau: a volcanic passive margin fragment?, *Geology, 23* (2), 137-140, 1995.

Operto, S., P. Charvis, F. Glangeaud, and J.M. Vanpé, P- and S-waves velocity structure of an oceanic crust from 3-component OBS data (abstract), *Ann. Geophys.,* 12, C22, 1994.

Paul, A., and F. Nicollin, Thin crustal layering in Northen France: Observations and modelling of the PmP spectral content, *Geophys. J. Int., 99,* 229-246, 1989.

Peirce, C., and P.J. Barton, Crustal Structure of the Madeira-Tore Rise, eastern North Atlantic - Results of a DOBS wide-angle and normal incidence seismic experiment in the Josephine Seamount region, *Geophys. J. Int., 106,* 357-378, 1991.

Powell, C.M., S.R. Roots, and J.J. Veevers, Pre-breakup continental extension in East Gondwanaland and the early opening of the eastern Indian Ocean, *Tectonophysics, 155,* 261-283, 1988.

Pringle, M.S., M. Storey, and J. Wijbrans, $^{40}Ar/^{39}Ar$ geochronology of mid-cretaceous Indian Ocean basalts: Constraints on the origin of large flood basalt provinces (abstract), *Eos Trans. AGU,* 75, Fall Meet. Suppl., 728, 1994.

Ramsay, D.C., J.B. Colwell, M.F. Coffin, H.L. Davies, P.J. Hill, C.J. Pigram, and H.M.J. Stagg, New findings from the Kerguelen Plateau, *Geology, 14,* 589-593, 1986.

Recq, M., D. Bréfort, J. Malod, and J.-L. Veinante, The Kerguelen-Isles (southern Indian Ocean): New results on deep structure from refraction profiles, *Tectonophysics, 182,* 227-248, 1990.

Rotstein, Y., R. Schlich, and M. Munschy, Structure and Tectonic of the Southern Kerguelen Plateau (Indian Ocean) deduced from seismic reflection data, *Tectonics, 11* (6), 1332-1347, 1992.

Royer, J.-Y., and M.F. Coffin, Jurassic to Eocene plate tectonic reconstructions in the Kerguelen plateau region, *Proc. Ocean Drill. Program, Sci. Results, 120,* 917-928, 1992.

Royer, J.Y., J.W. Pierce, and J.K. Weissel, Tectonic constraints on hotspot formation of the Ninetyeast Ridge, *Proc. Ocean Drill. Program, Sci. Results, 121,* 763-776, 1991.

Royer, J.Y., and D.T. Sandwell, Evolution of the eastern Indian Ocean since the Late Cretaceous: Constraints from Geosat altimetry, *J. Geophys. Res., 94,* 13755-13782, 1989.

Salters, V.J.M., M. Storey, J.H. Sevigny, and H. Whitechurch, Trace element and isotopic characteristics of Kerguelen-Heard Plateau basalts., *Proc. Ocean Drill. Program, Sci. Results, 120,* 55-61, 1992.

Sandwell, D.T., and W.H.F. Smith, ERS-1 geodetic mission reveals detailed tectonic structures (abstract), *Eos Trans. AGU,* 155, Fall Meet. Suppl., 728, 1994.

Schaming, M., and Y. Rotstein, Basement reflectors in the Kerguelen Plateau, south Indian Ocean: Indications for the structure and early history of the plateau, *Geol. Soc. Am. Bull.*, *102*, 580-592, 1990.

Schlich, R., M.F. Coffin, M. Munschy, H.M. Stagg, Z.G. Li, and K. Revill, Bathymetric chart of the Kerguelen Plateau, joint publication, Bur. of Miner. Resour., Canberra, Australia and Inst. de Phys. du Globe, Strasbourg, France, 1987.

Schlich, R., J.R. Delteil, J. Moulin, P. Patriat, and R. Guillaume, Mise en évidence d'une sédimentation de marge continentale sur le plateau de Kerguelen-Heard, *C.R. Acad. Sci. de Paris*, *272*, 2060-2063, 1971.

Schlich, R., et al., Kerguelen Plateau, *Proceedings of the Ocean Drilling Program, Initial Reports*, Ocean Drill. Program, College Station Texas, 1989.

Sinha, M.C., K.E. Louden, and B. Parsons, The crustal structure of the Madagascar Ridge, *Geophys. J. R. Astron. Soc.*, *66*, 351-377, 1981.

Spence, G.D., R.S. White, G.K. Westbrook, and S.R. Fowler, The Hatton Bank continental margin, I, Shallow structure from two ship expanding spread seismic profiles, *Geophys. J.*, *96*, 273-294, 1989.

Storey, M., R.W. Kent, A.D. Saunders, V.J. Salters, J. Hergt, H. Whitechurch, J.H. Sevigny, M.F. Thirlwall, P. Leat, N.C. Ghose, and M. Gifford, Lower cretaceous volcanic rocks on continental margins and their relationship to the Kerguelen Plateau, *Proc. Ocean Drill. Program, Sci. Results*, *120*, 33-53, 1992.

Storey, M., A.D. Saunders, J. Tarney, I.L. Gibson, M.J. Norry, M.F. Thirlwall, P. Leat, R.N. Thompson, and M.A. Menzies, Contamination of Indian Ocean asthenosphere by the Kerguelen-Heard mantle plume, *Nature*, *338*, 574-576, 1989.

White, R., and D. McKenzie, Magmatism at rift zones: The generation of volcanic continental margins and flood basalts, *J. Geophys. Res.*, *94* (B6), 7685-7729, 1989.

White, R.S., D. McKenzie, and R.K. O'Nions, Oceanic crustal thickness from seismic measurements and rare earth element inversions, *J. Geophys. Res.*, *97* (B13), 19683-19715, 1992.

Whitechurch, H., R. Montigny, J. Sevigny, M. Storey, and V.J.M. Salters, K-Ar and $^{40}Ar/^{39}Ar$ ages of Central Kerguelen Plateau basalts, *Proc. Ocean Drill. Program, Sci. Results*, *120*, 71-77, 1992.

Zelt, C.A., and R.B. Smith, Seismic traveltime inversion for 2-D crustal velocity structure, *Geophys. J. Int.*, *108*, 16-34, 1992.

P. Charvis, Observatoire Océanologique de Villefranche, UMR Géoscience Azur, ORSTOM, B.P. 48, 06230 Villefranche-sur-mer, France. (e-mail: charvis@ccrv.obs-vlfr.fr)

S. Operto, Ecole des Mines de Paris, Centre de Recherche en Géophysique, 35 rue Saint -Honoré, 77305 Fontainebleau, France. (e-mail: operto@geophy.ensmp.fr)

(Received September 7, 1995; revised March 29, 1996;
accepted May 24, 1996.)